SSSU 53
ISSN 0140 3818

UNIVERSITY OF SOUTHAMPTON

DEPARTMENT OF SHIP SCIENCE

FACULTY OF ENGINEERING AND APPLIED SCIENCE

VALIDATION OF A LIFTING SURFACE METHOD FOR MODELLING RUDDER-PROPELLER INTERACTION

by S.R. Turnock

Ship Science Report No. 53

April 1992

SSSU 53
ISSN 0140 3818

UNIVERSITY OF SOUTHAMPTON

DEPARTMENT OF SHIP SCIENCE

FACULTY OF ENGINEERING AND APPLIED SCIENCE

VALIDATION OF A LIFTING SURFACE METHOD FOR MODELLING RUDDER-PROPELLER INTERACTION

by S.R. Turnock

Ship Science Report No. 53

April 1992

VALIDATION OF A LIFTING-SURFACE PANEL METHOD FOR MODELLING RUDDER-PROPELLER INTERACTION

by

S.R.Turnock

Ship Science Report No. 53

University of Southampton

May 1993

SUMMARY

The validation of a method for modelling the interaction between a rudder and propeller is the subject of this chapter. A brief description is given of the process of successful validation of a CFD algorithm. The parallel algorithms of the PALISUPAN code are the basis of the lifting surface analysis carried out. Experimental results obtained from the wind tunnel test programme are used to validate firstly a lifting-surface model of a free-stream all-movable rudder (Rudder No. 2), secondly to model the open-water performance of the four-bladed propeller (modified Wageningen B4.40), and finally a representative rudder-propeller geometry. The representative geometry chosen was the mid-longitudinal separation of Rudder no. 2 (X/D=0.39) and propeller, with no lateral separation (Y/D=0.0), and the maximum height of the propeller tip coincident with the rudder tip Z/D=0.75.

The development of the interaction velocity field method is described. An aim of the validation exercise was to discover the minimum number of panels necessary to obtain reliable rudder and propeller force characteristics. Also, the minimum number of panels to adequately define the interaction velocity field was found. The minimisation of computational effort allowed the parametric studies, described in the following report, to be carried out within a reasonable time-scale.

TABLE OF CONTENTS

LIST OF FIGURES

LIST OF TABLES

NOMENCLATURE

Ai Area of panel i

A Angular rotation vector (ordered x, y and then z)

c Chord

C_D Non dimensional drag coefficient

C_f Coefficient of skin friction

C_l Local lift coefficient

C_L Non dimensional lift coefficient

Cp Pressure coefficient

Dij Body dipole panel j's influence at point i

F Body force vector

L Ratio of the distance from panel centroid to a point to that of the length of the largest panel diagonal

M Body moment vector

n unit surface normal vector

O Offset vector

P Pressure

P Pivot vector

r Radial distance between two points

Rn Reynolds number

S Scale vector

S_B Bounding body surface

Sij Body source panel j's influence at point i

S_W Wake surface

s semi-span

$U\infty$	free-stream speed
U	velocity vector
v	Disturbance velocity vector
Wik	wake dipole panel k's influence at point i
R,a,θ	Cylindrical coordinates
t,s	parametric arc-lengths along three-dimensional space curves
x,y,z	Cartesian coordinates
ρ	Density
Δt	Time step
ϕ	Disturbance potential
σ	Source strength
μ	Dipole strength
ω	angular velocity vector

1 INTRODUCTION

A propeller upstream of a ship rudder accelerates and rotates the flow onto the rudder. Additionally the ship rudder both blocks and diverts the flow arriving at the propeller.
The development and validation of a lifting-surface panel method for modelling the interaction between a rudder and propeller is the subject of this report.

A lifting-surface panel method has been developed for modelling both ship rudders and propellers(Turnock[1]). This is used to separately model the rudder and propeller. Their mutual interaction is accounted for by the use of a modified inflow velocity field. This technique is referred to as the Interaction velocity Field (IVF) method. Experimental results obtained from a wind tunnel test programme investigating ship rudder-propeller interaction (Molland & Turnock [2,3]) are used to validate:
1) a lifting-surface model of a free-stream all-movable rudder;
2) a four-bladed propeller;
3) a representative rudder-propeller geometry.

An all-movable rudder of rectangular planform with an effective aspect ratio of 3.0 and maximum thickness of 20% chord. This corresponds to model Rudder No. 2 used in the experimental test programme. The four-bladed modified Wageningen B4.40 propeller used in the wind tunnel tests was the basis for the lifting surface model propeller. Again, corresponding to the wind tunnel tests representative rudder-propeller arrangement chosen was the mid-longitudinal separation of rudder no. 2 (X/D=0.39) and propeller, with no lateral separation (Y/D=0.0), and the maximum height of the propeller tip coincident with the rudder tip (Z/D=0.75). Figure 1 is a schematic view of the wind tunnel test arrangement and indicates the relevant nomenclature. The rudder-propeller arrangement is considered to be representative of actual ship rudder-propeller geometries.

The interaction velocity field method's development is described. An aim of the validation exercise was to discover the minimum panelling density necessary to obtain reliable rudder and propeller force characteristics. Also, for the reasons of reducing computational costs, the number of points required to define the interaction velocity field was investigated. By

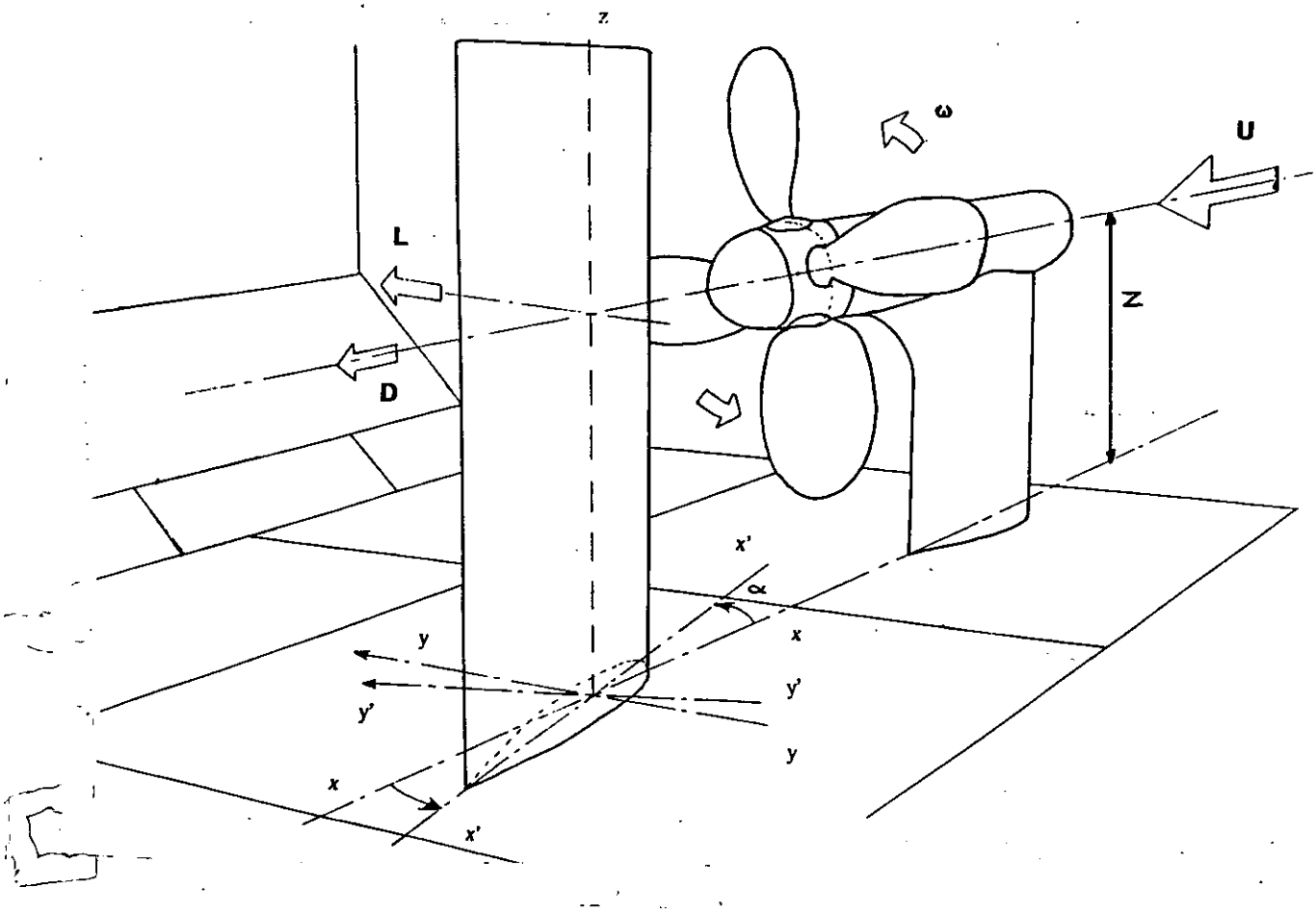

Figure 1 Schematic of rudder-propeller wind tunnel test arrangement

minimising the total computational effort it then becomes possible to carry out parametric and design studies of rudder-propeller interaction.

2 VALIDATION OF NUMERICAL ALGORITHMS

A mathematical model of a physical process generally involves a degree of approximation. In using such a model it is necessary to appreciate the confidence with which the model can be used. In the same way in which there is always error involved in the acquisition of experimental data, numerical modelling gives rise to uncertainty in the obtained answer. The process of validation attempts to quantify these uncertainties.

The precise definition as to what constitutes a validated CFD code is the subject of

debate at the present time. The process of code validation can be seen as a series of stages.

1) Verification of the code implementation against the underlying mathematical formulation. This is to ensure the code is free of error due to mistakes in expressing the mathematics in the particular computer language used. Ideally the comparison should be made against an analytic solution although often the comparison can only be made with other numerical codes.

2) Investigation of the independence of the solution from numerical parameters. The most common form of dependence is on the density of the grid of points at which the governing equations are solved. Normally, the number of grid points (or panels) is increased until the solution does not change. For iterative techniques which use a convergence criterion the dependence of solution on its value has also to be investigated.

3) Comparison of numerical and experimental data. This is the most tendentious area of code validation. As the majority of fluid dynamic codes are an approximation to the actual physics of the flow there will be differences between the experimental and numerical results. Experimental data should have a specified accuracy. This should then allow the difference between experiment and theory to be quantified. However, in many codes some degree of empiricism is used to adjust the numerical model to fit specific experimental data. The extent to which such an empirically adjusted model can be said to be valid for cases run at different conditions requires careful consideration.

In this work the aim has been to limit the amount of empiricism used in the modelling. This should then allow more confidence to be placed in the results obtained outside the conditions used for comparison. However, there will be differences between the numerical model and the experimental results which arise from the approximation of the Navier-Stokes equations by an inviscid, irrotational and incompressible formulation using discrete panels.

The verification of the lifting surface panel method against both analytic and other lifting surface solutions was described in (Turnock[1]). In this report a validation process

is carried out for the free-stream modelling of the rudder and propeller and then for their mutual interaction. A limited number of examples of solution convergence against panelling density are given. The convergence behaviour of panel methods having been well documented. Detailed comparison is made with the experimental data for a limited series of cases. In these it is shown that the method identifies the correct physical trends and thus can be used with confidence for interpolation between the values of experimental parameters tested and for a limited degree of extrapolation.

3 FREE-STREAM RUDDER PERFORMANCE

3.1 Introduction

A ship rudder, for the purpose of analysis, can be considered to be a low aspect-ratio wing. Difficulties arise when lifting-line theory is applied because of large cross-flow velocity components developed, especially at high incidence. Molland[4] developed empirical corrections to allow the lifting-line modelling of both semi-balanced skeg and all-movable rudders. To avoid such empiricism in modelling rudder-propeller interaction a lifting-surface panel method has been implemented. Various rudder test cases were run using the developed program and the results compared with the wind tunnel tests for a free-stream rudder. Comparisons were made for Rudder No. 2 which has a 1m span, chord of 0.667m and a constant NACA0020 section (t/c=0.2).

3.2 Lifting Surface Model of Rudder

The numerical definition of Rudder No. 2 specifies three identical NACA0020 sections, with ordinates taken from Abbott & Van Doenhoff[5], at heights of 0.0m, 0.5m, and 1.0m above the wind tunnel floor. The wake sheet trails downstream in the inflow direction. The flexible geometry definition allows both the number of span-wise and chord-wise panels (Nt, Ns), and the local panel density to be varied. Figure 2 shows three panelling arrangements for Rudder No. 2 each with a total of 400 panels: (a) shows 50 chordwise and 8 span-wise panels of uniform size; (b) shows 25 chordwise and 16 span-wise

uniform panels; and (c) 25 by 16 panels with sinusoidal clustering at the leading and trailing edge and rudder tip. The rudder model uses a reflection plane at the rudder root to account for the flow symmetry due to the wind tunnel floor. This neglects the wind tunnel boundary layer and approximates to the flow symmetry which occurs on a ship due to the presence of the hull.

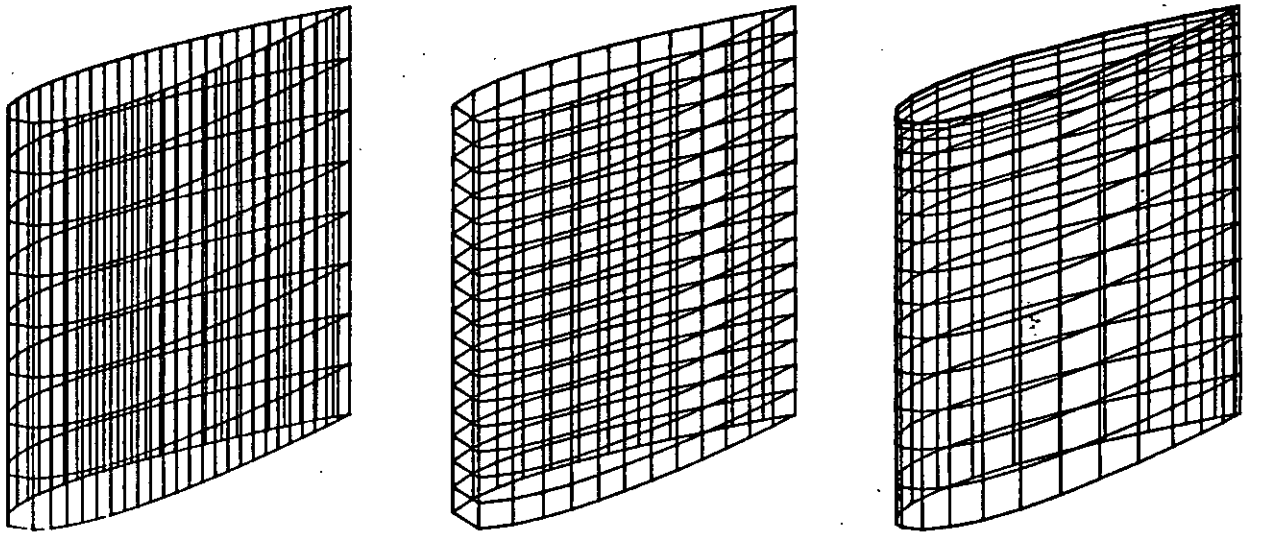

Figure 2 Three panelling arrangements for Rudder No. 2

Different rudder incidences are modelled by applying a rotation about the z-axis with the pivot point set at 200mm from the leading edge. This corresponds to the location of the rudder stock on Rudder No. 2.

Changing the scale vector S allows the experimental Rudder No.'s 3,4,5 and 6 to be generated from the same basic configuration.

3.3 Comparison of Model and experiment

For a rudder incidence of 9.6^0, sensitivity studies were carried out into the effect of panel distribution, local panel density, and total number of panels. The maximum number of panels used was 400, which corresponds to the maximum available on the 4 transputer

Ship Science system (SSTS) upon which the flow solver was developed. Figure 3 shows the lift C_L and drag C_D variation against the total number of panels for two cases

1) a constant number of spanwise panels, Ns=8

2) a constant number of chordwise panels, Nt=25.

These figures were obtained with sinusoidal panel clustering at the leading edge, trailing edge and tip. The straight line represents the wind tunnel experimental value. It can be seen that there is only a limited convergence with increasing number of spanwise strips. However, increasing the number of panels per spanwise strip causes a gradual convergence towards the experimental value. This is due to the increased panel resolution around the area of rapidly changing curvature at the leading edge. The drag is sensitive to small changes in panel geometry which accounts for the fluctuation about the experimental value. Four hundred panels is not sufficient to converge the value of lift or drag, but it was considered to be good enough for assessing the manoeuvring performance and for finding parametric trends. It should be noted that the lifting-surface panel method only models potential flow. Therefore, because of the absence of a viscous boundary layer the lift will be overpredicted and drag underpredicted.

For the investigation into the sensitivity of the final solution to total number of body panels the wake length was held constant at a value of 5 rudder chords. Each wake strip was equally divided into 50 panels. This value was chosen because, as shown in Figure 4 (Nt=25, Ns = 16), after a wake length of about 4 rudder chords the value of lift and drag converged. A constant panel density of 10 per rudder chord was used. For the cases described a convergence criterion was applied that the maximum non-dimensional trailing edge pressure load was less than 0.01.

$$\Delta Cp_{t.e.} < 0.01 \qquad [1]$$

Figure 5 compares the surface pressure values for this numerical test case with experimental values. The numerical test had 50 chordwise by 8 spanwise panels with sinusoidal clustering. A linear interpolation was applied to the theoretical values so that the spanwise location of theory and experiment corresponded. The lifting-surface values closely follow the form of the experimental points although the absolute value of pressure is always

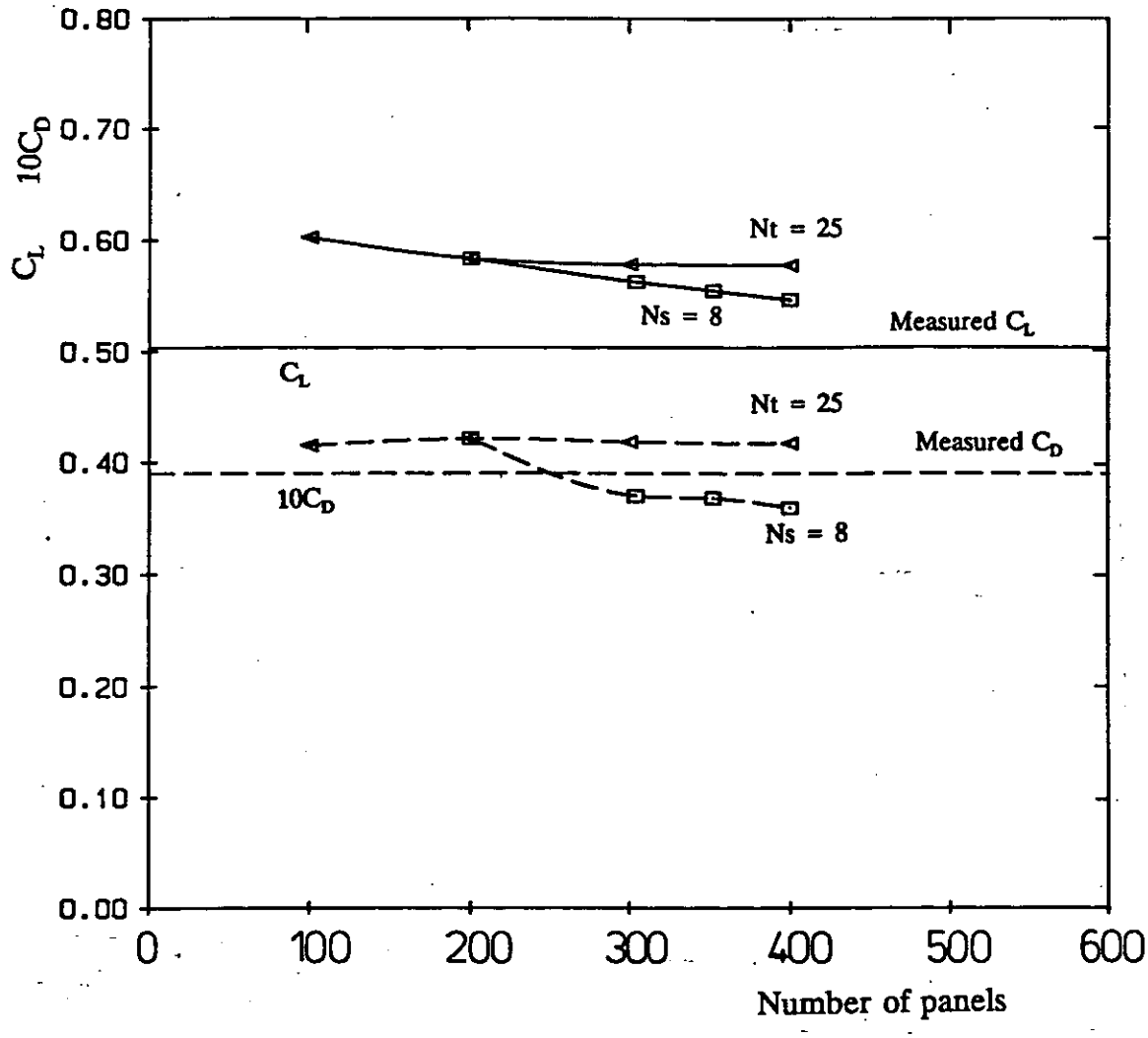

Figure 3 Variation of predicted rudder lift and drag with the total number of surface panels

overpredicted by the lifting-surface. At the spanwise section closest to the rudder root the lifting surface values are significantly larger. It is thought likely that this is due to the boundary layer flow along the wind tunnel floor which reduces the inflow velocity near the wall leading to reduced pressures and reducing the effective aspect ratio of the rudder. Also, at the spans nearest the rudder tip there is a divergence between experiment and lifting-surface towards the trailing edge of the suction side. This is probably due to the presence of a tip vortex (Molland[1]). The presence of the trailing vortex is indicated by the relatively high negative Cp values on the rearward portion of the suction side of the rudder. The effect is not modelled by the lifting-surface panel method. Molland obtained good prediction of the tip vortex using an empirical relationship for the tip vortex strength.

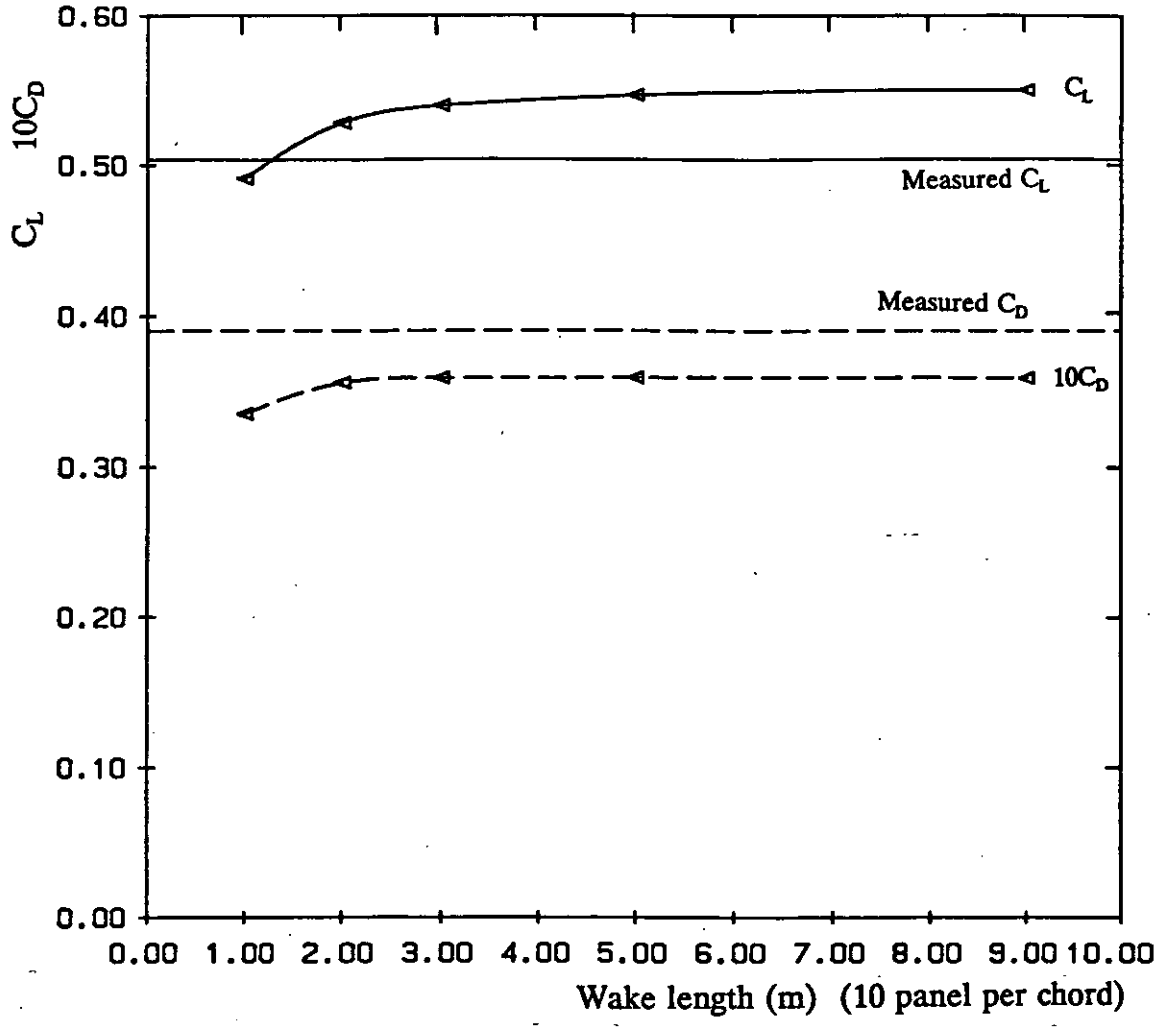

Figure 4 Variation in rudder lift and drag with increase in wake length

Chordwise integration of the surface pressure allows the local sectional lift coefficient C_l to be evaluated. For a rudder incidence of $+9.6^o$, Figure 6 compares the spanwise distribution of local lift for the experimental and lifting-surface result. Overall a good comparison is obtained. As noted in the surface pressure comparison the lifting surface overpredicts the pressure difference and hence lift. The difference is due to a combination of viscous effects and the restriction of surface panels to 400. The development of the viscous boundary layer alters the effective shape of the aerofoil and hence surface pressure distribution thus decreasing lift and increasing drag. The effect of the shedding of a vortex from the square edged rudder tip is clearly seen in the experimental result. It induces a characteristic hump to the load distribution close to the tip. For the purposes of rudder-propeller interaction modelling this effect has been neglected. Although it is of significance,

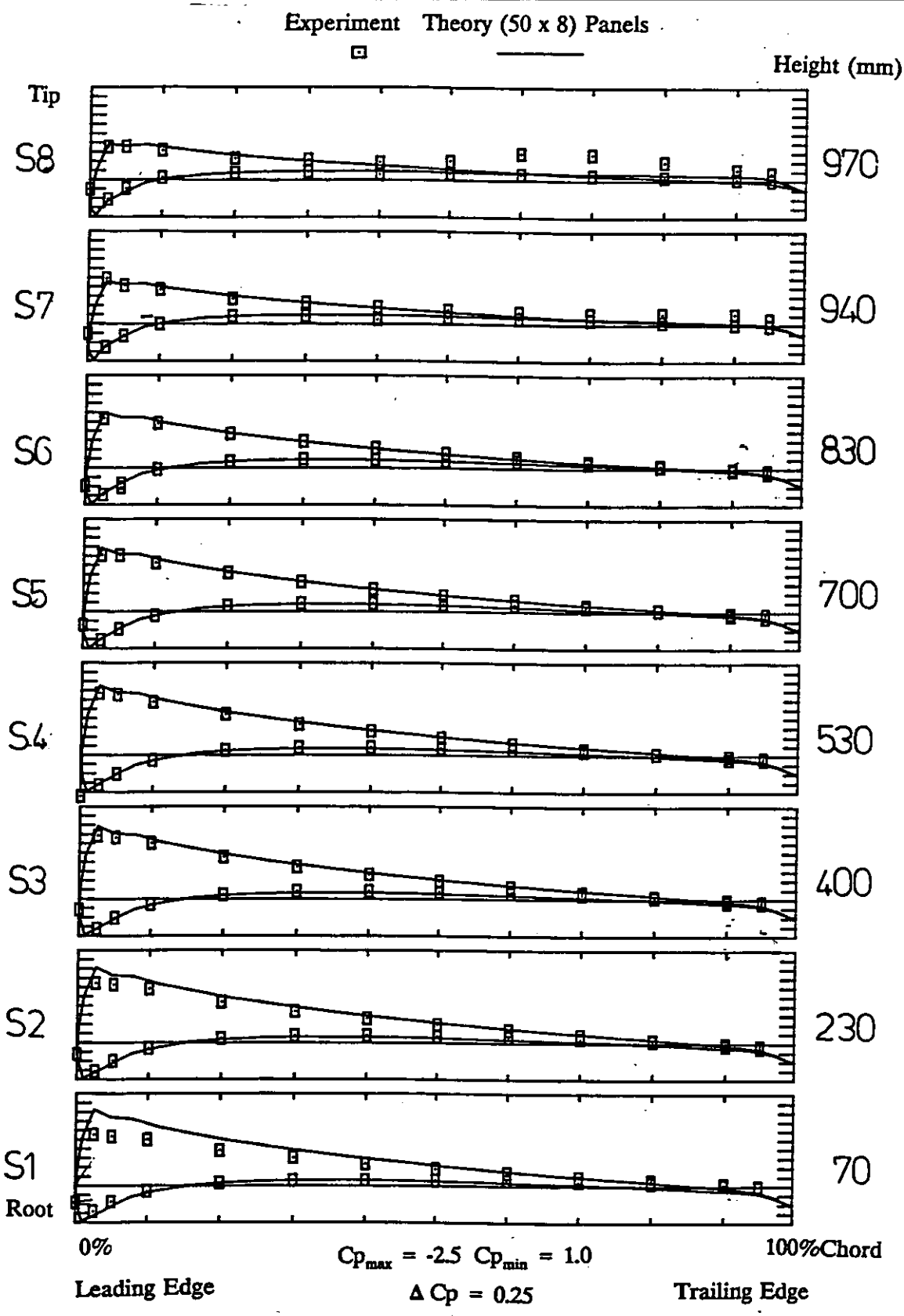

Figure 5 Comparison of experimental and numerical chordwise pressure distributions at 8 spanwise positions for Rudder No. 2 at $+9.6^{o}$

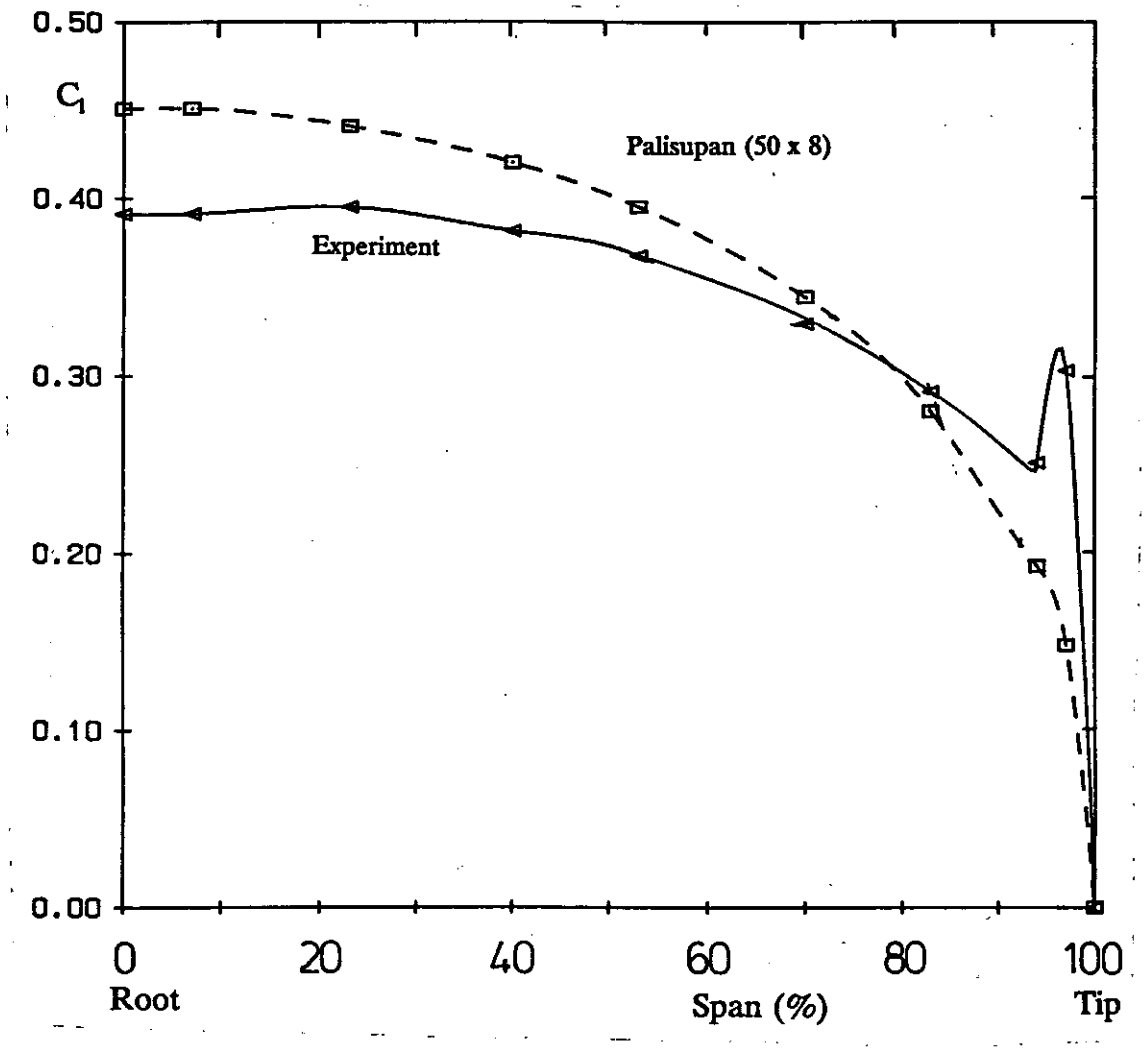

Figure 6 Comparison of experiment and theory for the variation in spanwise distribution of local lift coefficient C_l for rudder no.2 at 9.6^o

especially at high incidence, it was considered unlikely to influence the overall trends.

Finally, Figure 7 compares C_L, C_D, CP_s, and CP_c for a range of rudder incidence between -25^o and 25^o up to and including stall. As would be expected for an inviscid method the gradual onset of stall and subsequent reduction in lift at higher incidence is not predicted. However, the overall comparison of lift and drag characteristics is good. The numerical lift curve slope at 0^o is 10% greater than the experimental value. The chordwise position of centre of pressure is fairly well predicted but because of the overprediction of lift by the lifting-surface method and the physical presence of a tip vortex the numerical prediction of the spanwise centre of pressure is about 5% of span nearer the root. As

mentioned previously, the difference is mainly due to neglecting the effect of the boundary layer on the pressure distribution (viscous pressure drag), tip vortex effects, the effective aspect ratio being less than twice the geometric aspect ratio, and the flat plate assumption for skin friction drag.

3.4 Velocity field ahead of rudder

The flow upstream of a rudder is affected by its presence and a knowledge of this upstream influence is necessary for determining the influence of the rudder on the propeller. Using the solution of the lifting-surface the velocity field upstream of the rudder can be obtained by the summation of all the individual velocity influences due to the body source/dipole panels and the wake dipole panels. This process defines an interaction velocity at any point in the field around the rudder. The total velocity at any point is the sum of this interaction velocity and the inflow velocity. To illustrate this, Figure 8 shows a velocity vector plot at a span of 0.5m around Rudder No. 2 at an incidence of 9.6^{o}. The characteristic upwash upstream of the rudder and flow acceleration around the rudder upper surface can be seen. The flow within the rudder was found to be at the free-stream value which indicates that the internal potential field is constant and equal to zero as required by the perturbation potential theory. The velocity field was generated by finding the velocity on a regular mesh of points. Close to the body surface there are localised effects due to the modelling of the surface as constant strength quadrilateral panels.

To account for the interaction of the rudder at the propeller plane the interaction velocity is found on a circular disk of points. The location of the circular disk corresponds to the actual location of the propeller relative to the rudder. Circumferentially averaging the velocity of points at a given radius generates the spatial average inflow to the propeller. It was found that a minimum of 10 radial and 20 circumferential points gave adequate resolution of an average velocity field. As an illustration of this process for modelling the interaction Figure 9 shows the radial variation in average axial velocity for three rudder-propeller longitudinal separations corresponding to $X/D = 0.30, 0.39$, and 0.52. The greatest drop off in axial velocity occurs at the propeller hub ($r < 100$mm). As expected, the smaller the separation the greater the velocity defect. The variation in the average radial and

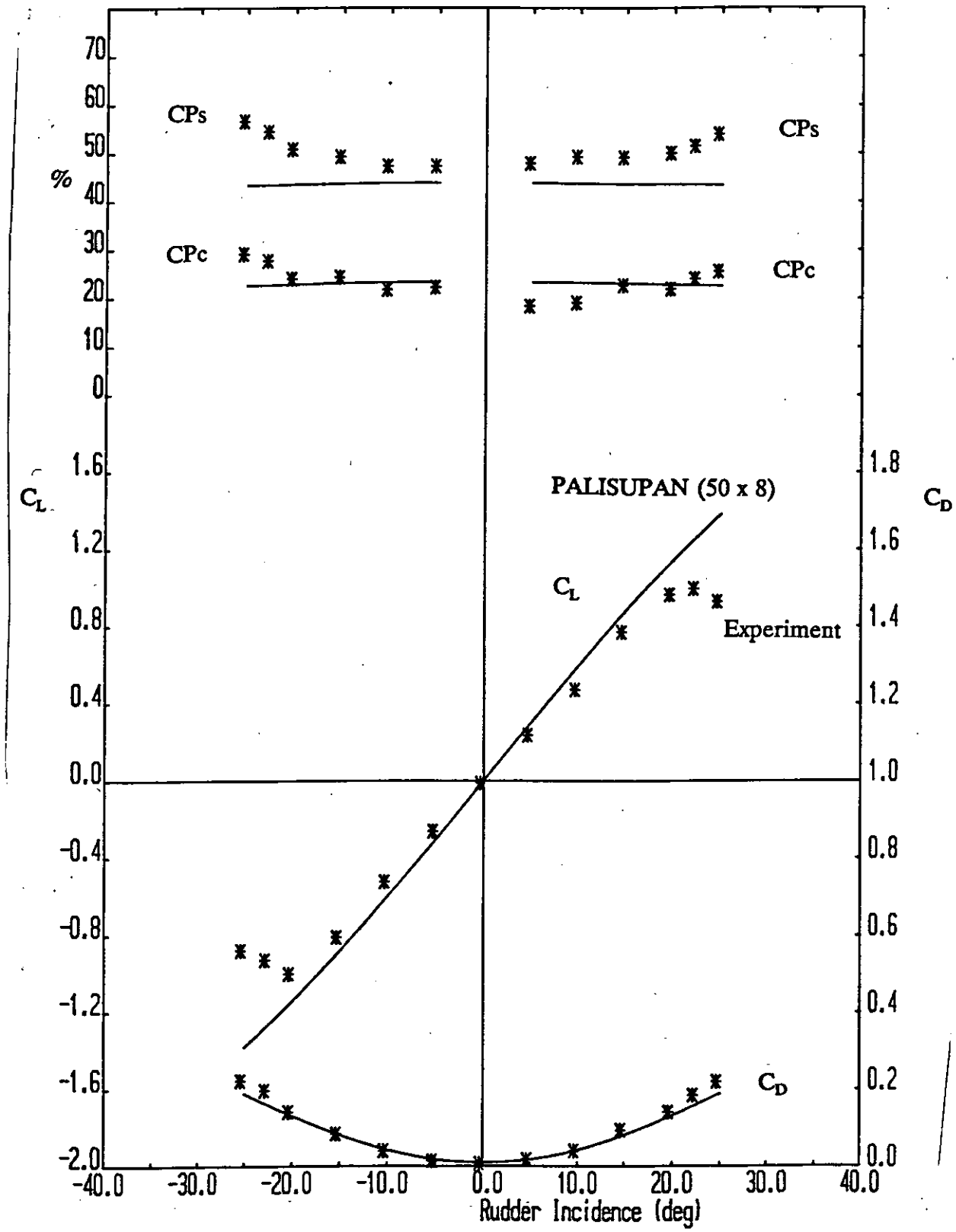

Figure 7 Comparison of lifting-surface and experimental lift, drag and centre of pressure characteristics for rudder no. 2 in free-stream

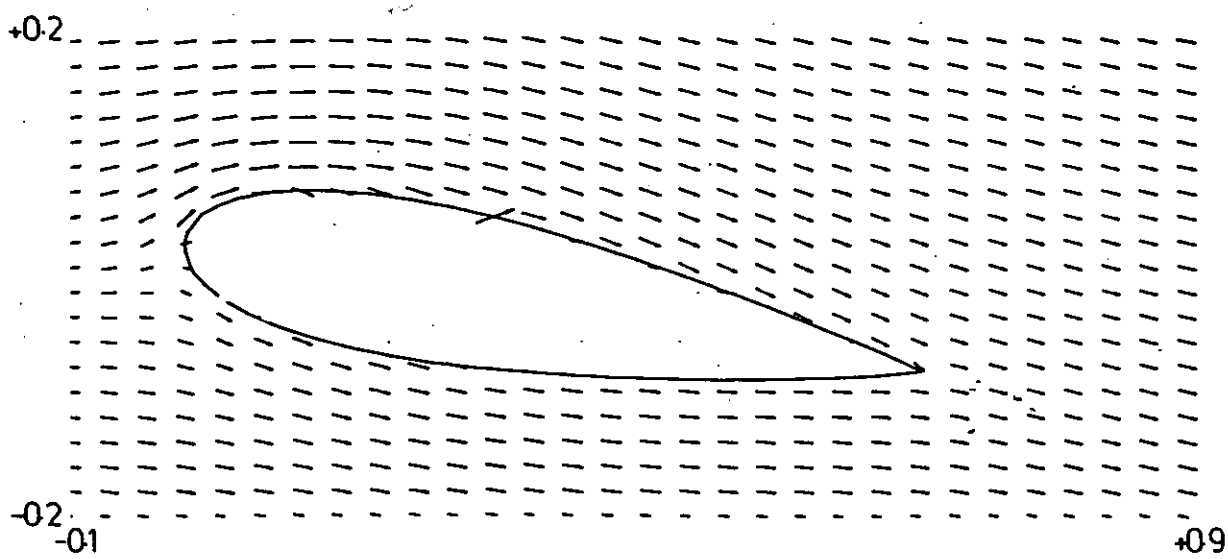

Figure 8 Velocity field at mid-span of Rudder No. 2 at incidence of 9.6^{o}

circumferential components of velocity are small $Vr < 0.25$m/s and $Vw < 0.05$m/s for a free-stream velocity of 10m/s and can be neglected when modelling the interaction. It should be noted that these components arise from the asymmetric location of propeller axis ($Z=0.6$m) relative to the flow over the rudder.

3.5 Summary

The comparison of experimental and lifting-surface results is satisfactory for rudder incidence up to stall. The method does not predict tip loading due to the shed vortex or the effect of a viscous boundary layer and wake. Bearing the above restrictions in mind and the limitation on the number of panels available it is considered that the prediction of lift-curve slope within 10% of the experimental value is acceptable for the purposes of investigating rudder-propeller interaction. The results can be improved through the use of empirical corrections for more detailed study of rudder performance but would then restrict the use of the method.

The circumferentially averaged interaction velocity field for use as a propeller inflow can be adequately generated from 200 velocity field points.

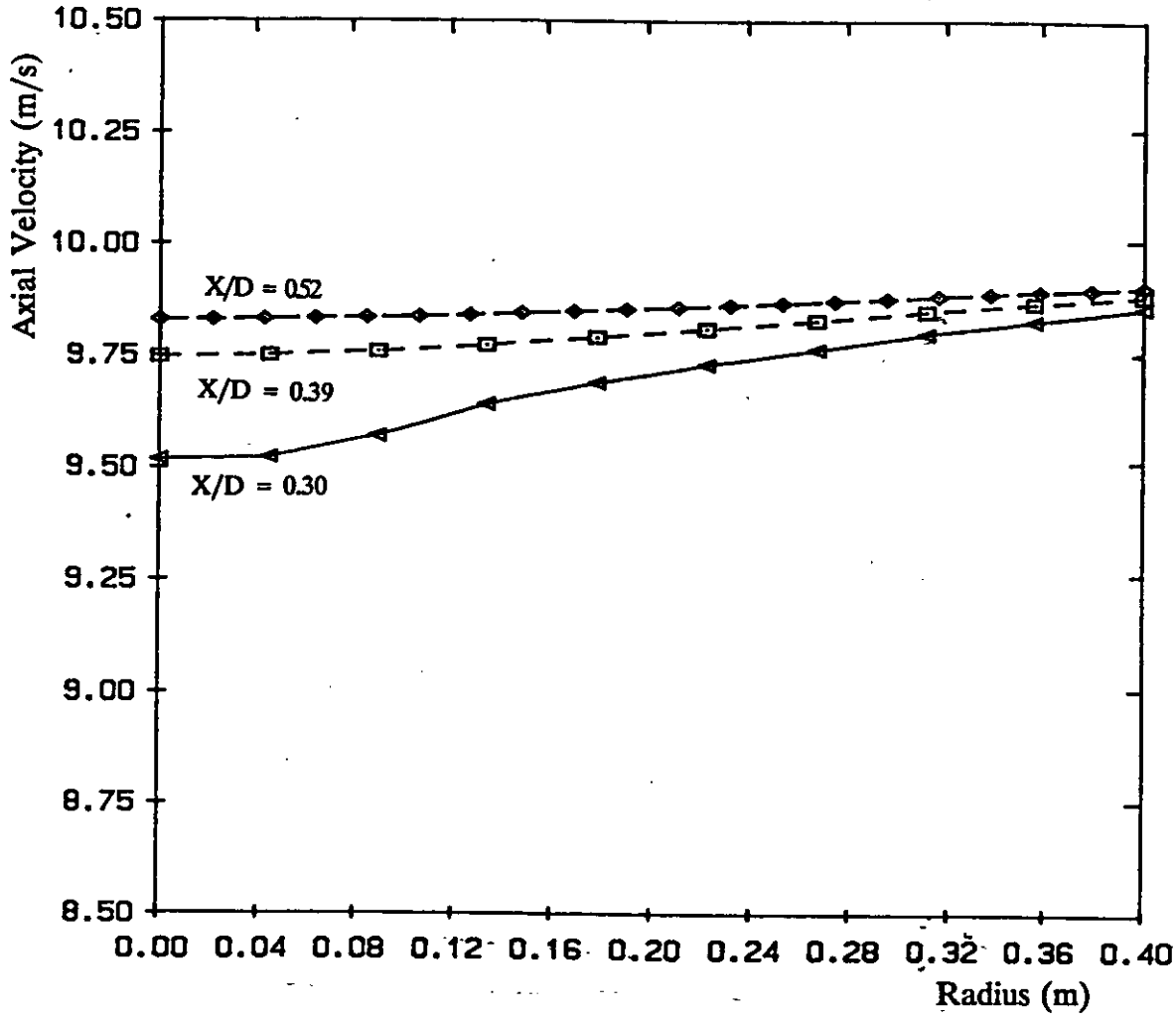

Figure 9 Effect of longitudinal separation on circumferentially averaged velocity upstream of Rudder No. 2

4 OPEN-WATER PERFORMANCE OF PROPELLER

4.1 Introduction

An important part of the developed interaction velocity field method is the accuracy with which the velocity field downstream of the propeller can be modelled. In order to obtain this velocity field it is first necessary to validate the open-water performance of the lifting-surface code against the free-stream tests of the experimental propeller. The propeller and hub geometry used for the lifting-surface model exactly correspond to those used in the experimental investigation. However, the influence of the ground board (reflection plane)

cannot be included as this would result in a spatially varying propeller inflow. Modelling this requires a time accurate model of all four propeller blades. This is feasible with the current formulation but would require large computational effort due to the need for extra surface panels and modelling at different angular positions. For similar reasons the propeller support structure present in the wind tunnel tests is ignored. A quasi-steady model which assumes an identical flow across all four blades has therefore been used.

4.2 Lifting surface model of propeller

The whole four-blade propeller and boss geometry is rotationally symmetric. Therefore, only one blade and a quarter segment of the boss need be modelled. The overall geometry is split into two components a non-lifting body (cylindrical boss) and lifting-surface (blade).

The numerical definition of the modified Wageningen B4.40 blade that was used to NC machine the model propeller blade was also used to generate sections at different radii out along the propeller blade for creating the surface panel data. The use of the same base propeller data ensures an identical geometry between lifting-surface model and experiment. The method developed also permits any standard table of propeller offsets to be used to generate a numerical model. The propeller pitch can be set at this stage by altering the angle of rotation of the blade about its generator. Figure 10 shows three projections and an isometric view of the model propeller blade section definition. The trailing wake sheet is specified as lying on a helical surface following a given pitch for each section.

Maitre[6] found, especially at high propeller loading, that modelling of the boss was necessary to obtain the correct blade load distribution. For this reason the final numerical model includes the boss. The design profile of the boss is identical to that used in the wind tunnel model except the upstream cylindrical section is shortened to increase the panelling density around the blade root. At the blade root-boss intersection to prevent numerical problems a correct matching of the geometry is required. The quarter segment of the body was set on a helical surface with the geometry pitch of the blade root. To obtain a smooth spline through the boss-blade interface region it was found necessary to use the elliptic grid

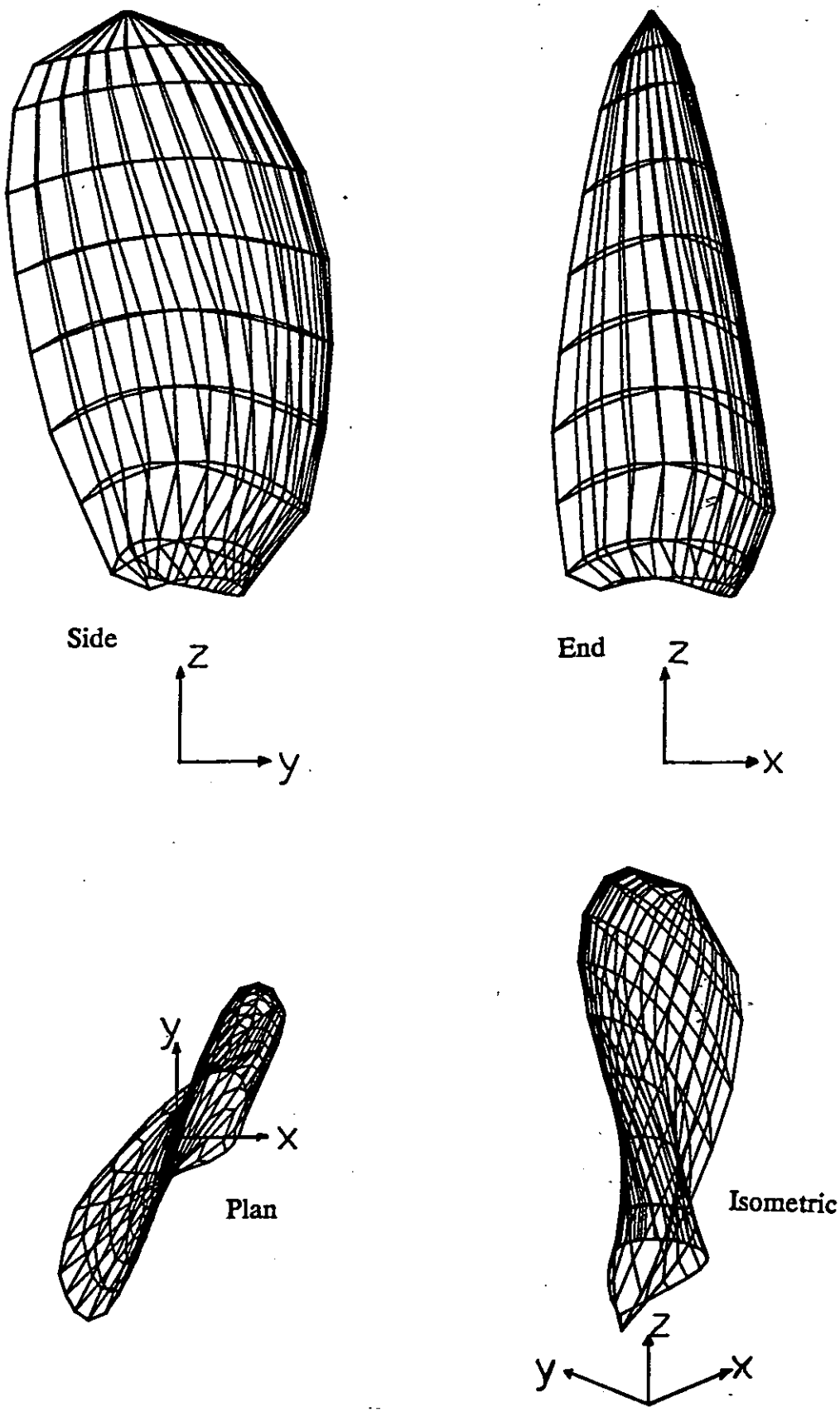

Figure 10 Three projections and isometric view of modified Wageninegn B4.40 propeller surface definition

generator described in Appendix C. Figure 11 shows the elliptically refined grid before fitting around a helical surface. In all, six curves were used to define the boss. The final surface definition geometry is shown, in plan and end on, in Figure 12.

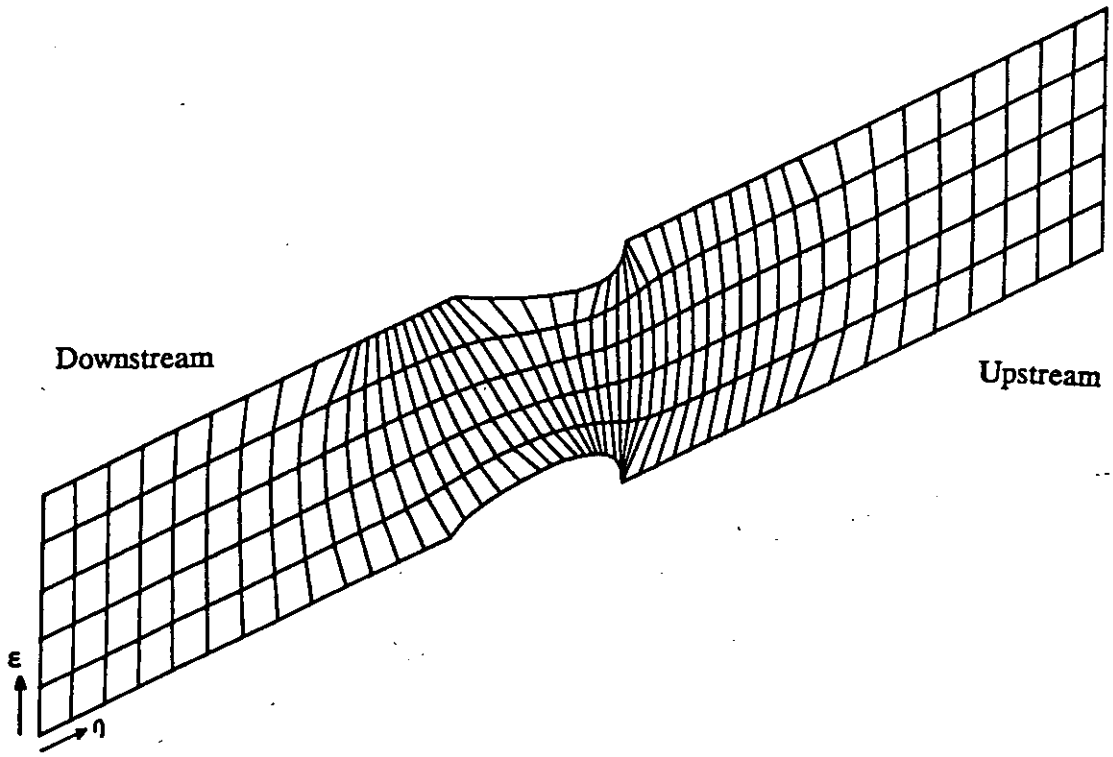

Figure 11 Elliptically refined grid for boss definition

Figure 13 is an isometric view looking upstream. The complete propeller and boss geometry is shown with 100 boss and 300 blade panels. All the image panels, 1200 in total, are shown using dotted lines.

4.3 Comparison of model and experiment

The basic model consisting of 25 by 4 boss panels and 25 by 12 blade panels, was run for a range of advance ratios between 0.2 and 1.0. A constant wind-speed condition equal to the experimental test speed of 10m/s was used. The different advance ratios were obtained by altering the propeller rate of revolution. Figure 14 compares the propeller thrust, torque and efficiency characteristics (K_T, K_Q, and η) between the surface panel model and experimental and Wageningen data, for a pitch ratio setting of P/D=0.95. As an initial first step for all the advance ratios tested the wake pitch at all sections was set equal to the

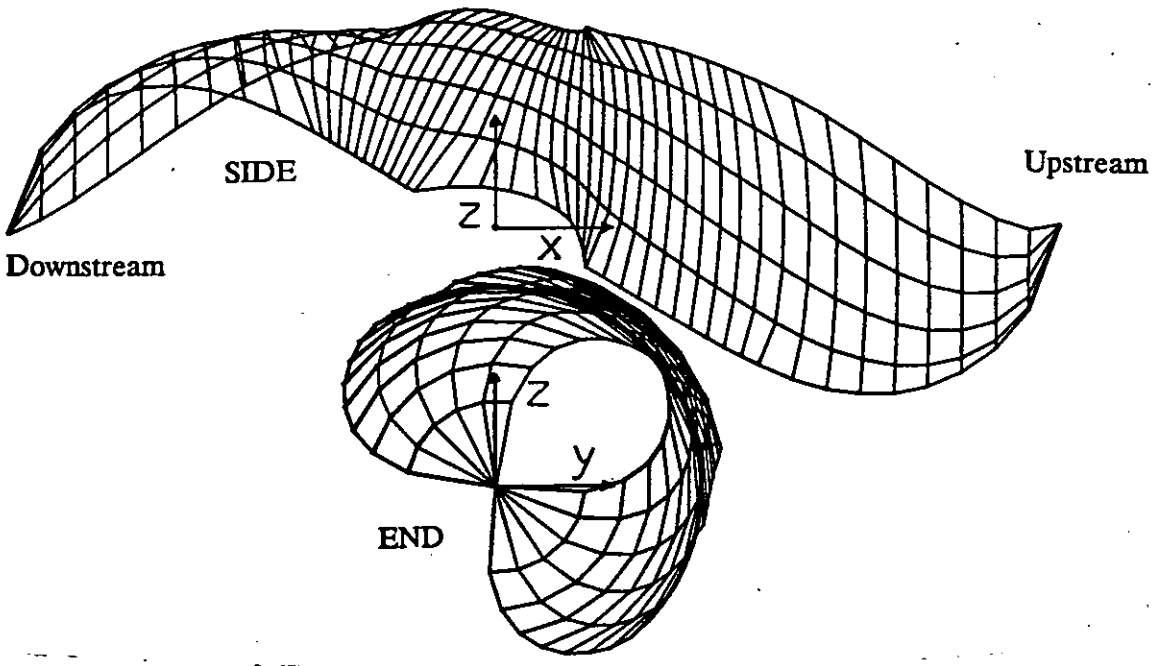

Figure 12 Plan and end view of boss surface definition

geometric pitch of the corresponding blade section. It can be seen that the efficiency gives good agreement but both thrust and torque are overpredicted. There are three main reasons for this:

1) the radial variation in actual wake pitch is important in determining the actual thrust/torque of a given blade section and the geometric pitch especially at low J, is a considerable over-prediction of the actual wake pitch which will result in higher blade loading;

2) the potential formulation neglects viscous effects (i.e. viscous pressure drag) which become especially important at low advance ratio when there is the possibility of stall/separation across areas of the blade;

3) the relatively low number of surface panels available for modelling the blade and boss.

Sensitivity studies were carried out into the panelling arrangement on the propeller blade alone. Table 1 shows the influence of total number of panels and the relative number of panels in the chordwise (Nt) and spanwise (Ns) directions on the propeller thrust coefficient at an advance ratio J of 0.35. It can be seen that the propeller, as opposed to the rudder, is more sensitive to the number of spanwise strips. Increasing the number of

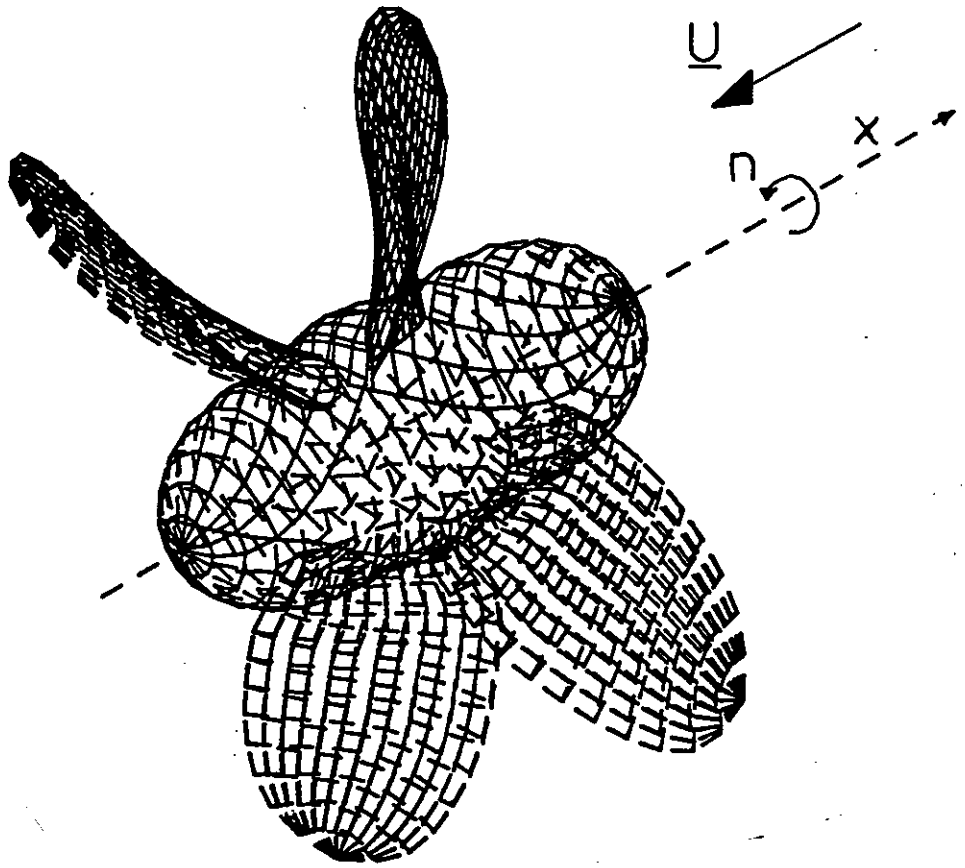

Figure 13 Isometric view upstream of 400 panel model of propeller blade and boss, also showing image panels(1200)

Table 1 Sensitivity of blade thrust coefficient to panelling arrangement for J=0.35

Total Number of Panels	100	200	300	400	296	360	392
	Variation with Ns				Variation with Nt		
Panel distribution(NtxNs)	25x4	25x8	25x12	25x16	37x8	45x8	49x8
Thrust Coefficient K_T	0.352	0.348	0.341	0.337	0.347	0.347	0.347

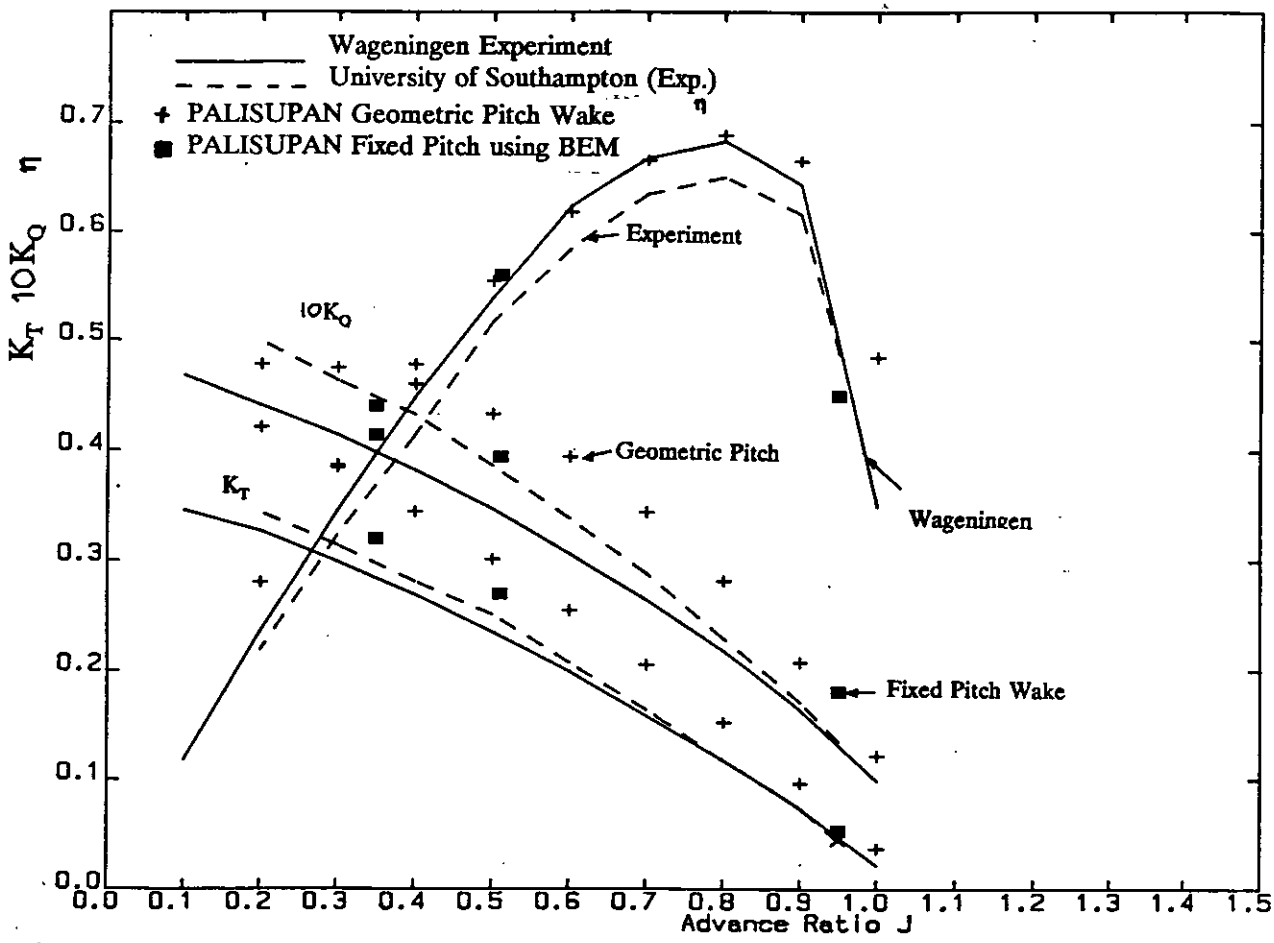

Figure 14 Comparison of model, experiment and Wageningen propeller characteristics

chordwise panels for a fixed number of strips has relatively little effect. It was found that, due to the asymmetric shape of the back and face of the propeller blade, a constant panel size rather than sinusoidal clustering gave the best result.

The effect of the total wake length on the performance of the propeller blade was quite marked, as is tabulated in Table 2. These values are for propeller blade thrust at a J of 0.35 and with 25 wake panels per metre at the propeller geometric pitch of 0.95. It can be seen that the thrust decreases with increasing wake length. Due to the curved nature of the wake the density of wake panels influences the wake thrust. It was found that a panel density of at least 25 panels per metre of wake was required for convergence. For a fixed wake downstream length of 2000mm, increasing the number of wake panels from 25 to 100

reduced the propeller thrust by 1.5%. At present the number of wake panels per strip is limited to 100 and therefore the maximum possible wake length was restricted to 4000mm. Maitre[6] carried out a similar exercise and used a wake length of 8 radii. Therefore, a length of 10 radii(4000mm) was deemed acceptable.

Table 2 Effect of wake length on propeller thrust

Wake length	Number of panels	Propeller Thrust K_T
1000mm	25	0.345
2000mm	50	0.341
4000mm	100	0.337

The adaption of a propeller's wake to follow the stream surface which gives zero pressure loading across the wake is fraught with difficulties. The principal source of these problems is the non-physical modelling of the wake as an infinitely thin sheet of dipole panels. Recently, Maitre[6] demonstrated that wake adaption for a lifting-surface panel method would converge to a physically realistic solution. However, constraints based on empirical evidence were still applied in the region close to the blade root. Lee[7] used a fixed wake shape developed from empirical measurements and numeric analysis to obtain close agreement. In this work the structure of the wake is important not only in determining the correct flow over the propeller but also in specifying the velocity field downstream of the propeller for use as an inflow to a rudder.

The process of wake adaption is computationally intensive involving the regeneration of the influence coefficient matrix and iterative solution after each wake adaption. Maitre[6] found that at least 20 iteration cycles were required to achieve convergence. In this work, due to the current limitations on body surface and wake panel numbers it was found that the method was unstable except for very short total wake lengths. Therefore, for the modelling of rudder-propeller interaction it was decided to use a fixed wake. The specification of the wake pitch at a given radius was based on the blade-element momentum results for axial and

circumferential velocity at the propeller plane derived by Molland[8] for the velocity downstream of the propeller. These were used to specify a wake pitch at a given radius. Figure 15 shows the radial distribution of wake pitch for the three experimental advance ratios of 0.35, 0.51, and 0.95 tested. It was found that using these pitch ratios improved the agreement between experiment and theory, especially at the lower advance ratio. The improved value of thrust, torque and efficiency are plotted on Figure 14 for comparison with the values obtained with a fixed geometric pitch. The sensitivity of propeller thrust and torque to wake pitch is demonstrated in Table 3. This shows the effect of different values of a radially constant wake pitch for an advance ratio of 0.35. It is interesting to note that the pitch of 610mm corresponds to the average pitch for the radially varying pitch. The fixed wake shape has no downstream radial contraction applied.

Table 3 Effect of a fixed pitch wake on propeller characteristics at J=0.35

Fixed Wake Pitch	Thrust K_T	Torque K_Q
823mm	0.333	0.0424
750mm	0.326	0.0420
700mm	0.319	0.0418
610mm	0.306	0.0411
575mm	0.299	0.0407

It is accepted that the specification of the propeller wake as either a radially constant 'average pitch' or radially varying pitch is a simplistic representation. However, as shown in the next section, the downstream velocity field was deemed acceptable given the constraints on the number of body and wake panels. It is expected that using a larger transputer array to carry out a wake adaption a more realistic wake shape can be obtained within a reasonable time-scale. Also, if at a future date L.D.A. measurements are carried out such information could be used to further enhance the wake model.

In Figure 16 the radial circulation distribution for three advance ratios of 0.35, 0.51

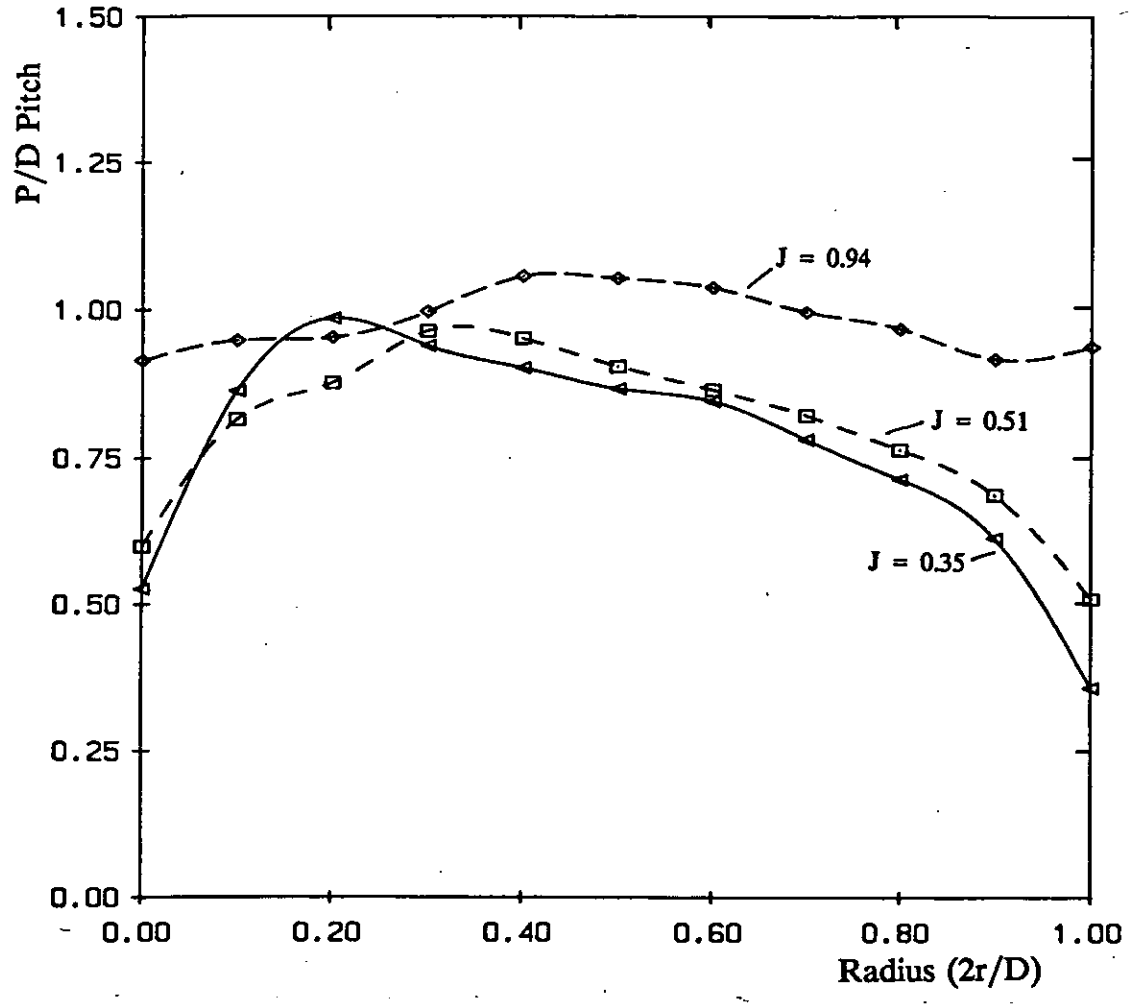

Figure 15 Radial variation of wake pitch for three advance ratio

and 0.95 are shown. Also plotted is the circulation distribution for the blade alone without the hub. It is interesting to see the effect of the hub holding up the value of circulation near the root and demonstrates the need for modelling of the hub geometry.

Chordwise surface pressure distributions for 8 radii are plotted in Figure 17 for the four circulation distributions shown in Figure 16. The pressure coefficients are non-dimensionalised in terms of the local velocity not the inflow velocity. That is

$$Cp = \frac{U_o \cdot U_o - U_t \cdot U_t}{U_o \cdot U_o} \qquad [2]$$

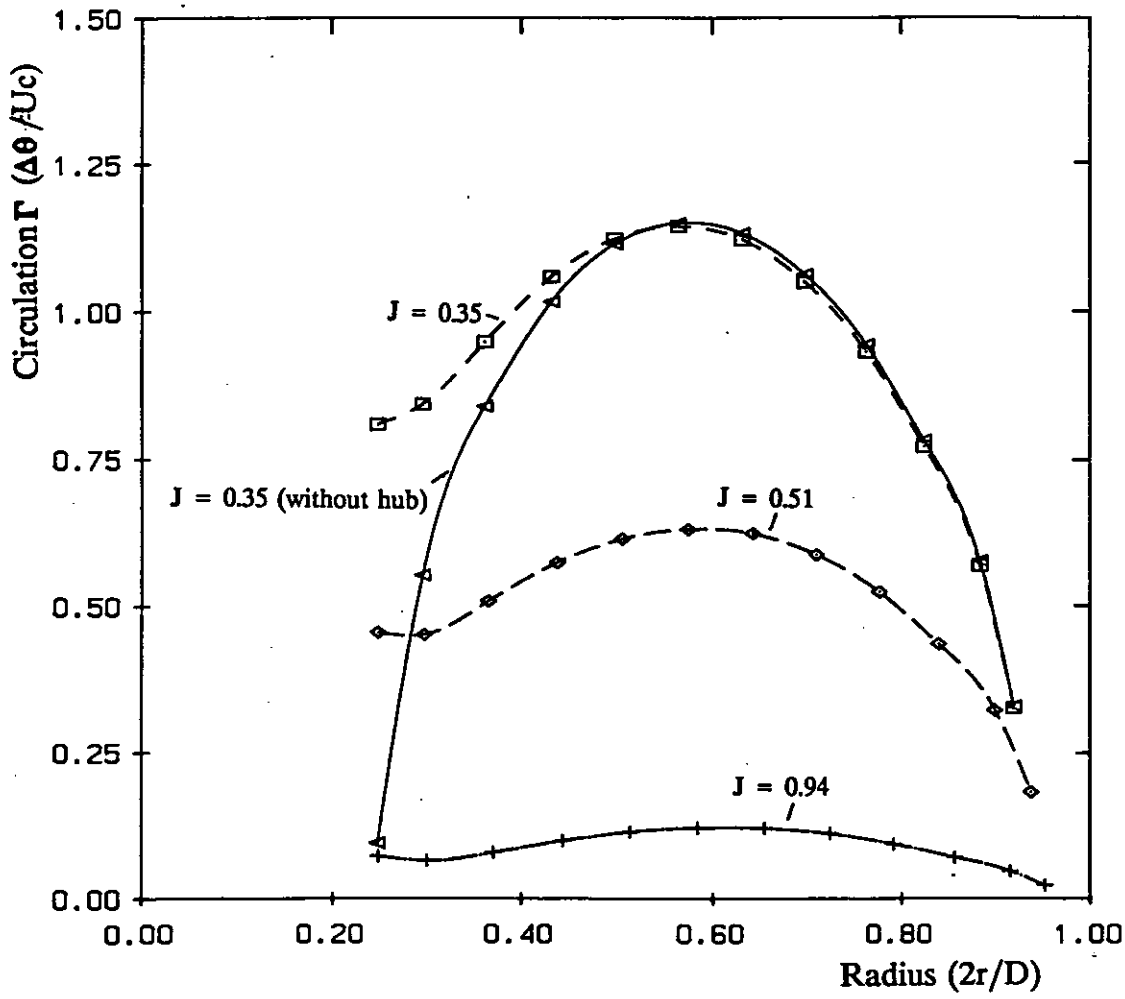

Figure 16 Radial distribution of circulation on propeller blade

where U_t is the surface panel velocity, U_0 the local velocity which is equal to:

$$U_0 = U_\infty + r \times \omega \qquad [3]$$

It is interesting to compare in Figure 17 the pressure distributions at the root for J of 0.35 with and without the boss. It is thought that the heavy loading at the blade root may be indicating that the flow is actually stalled or separated in that region and explain some of the discrepancy in thrust between experiment and lifting-surface model. The effect of decreasing advance ratio is seen with the local loading for each section gradually increasing.

The corresponding hub strip pressure distributions for an advance ratio of 0.35 are

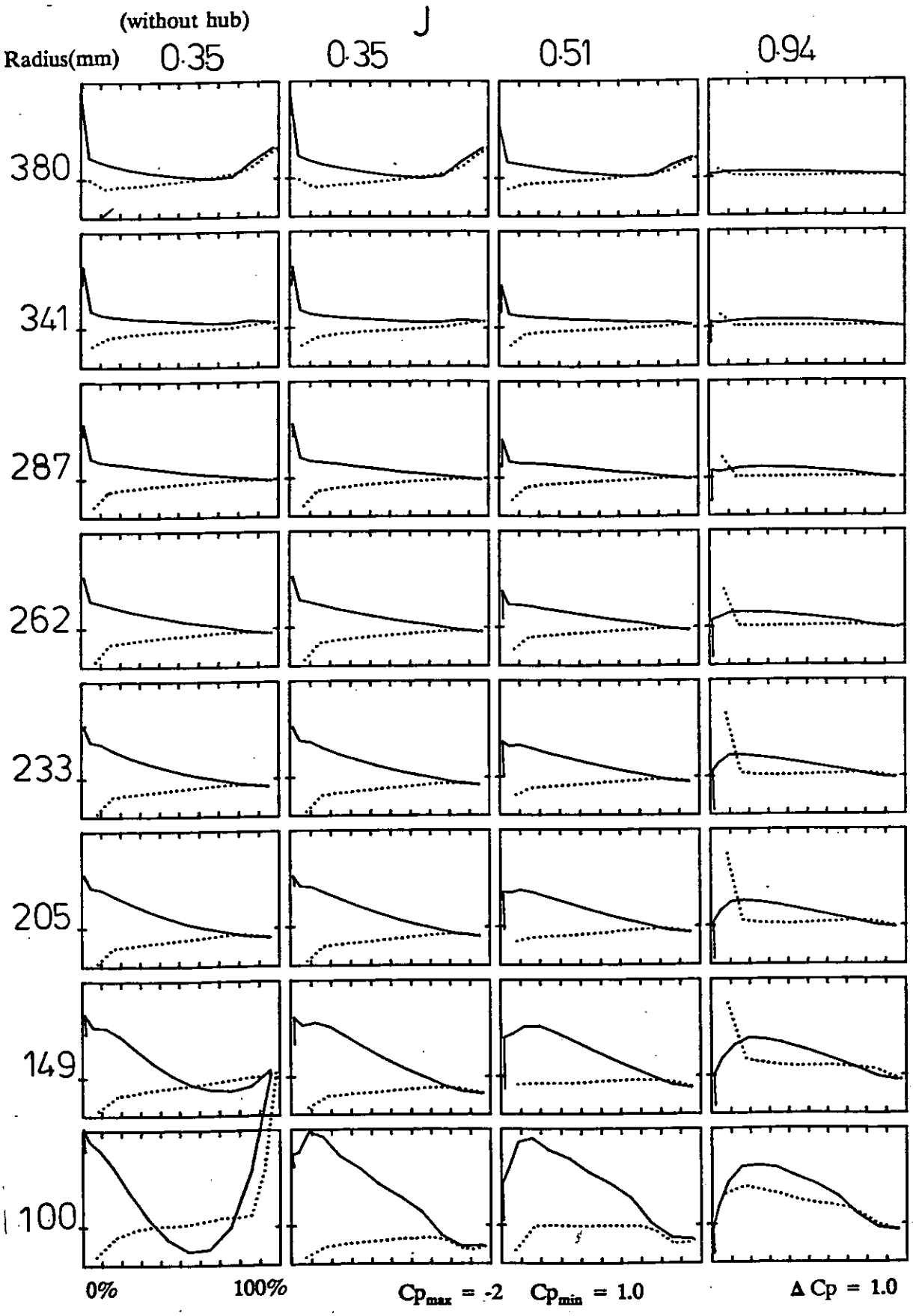

Figure 17 Chordwise pressure distributions for 8 radii on propeller blade

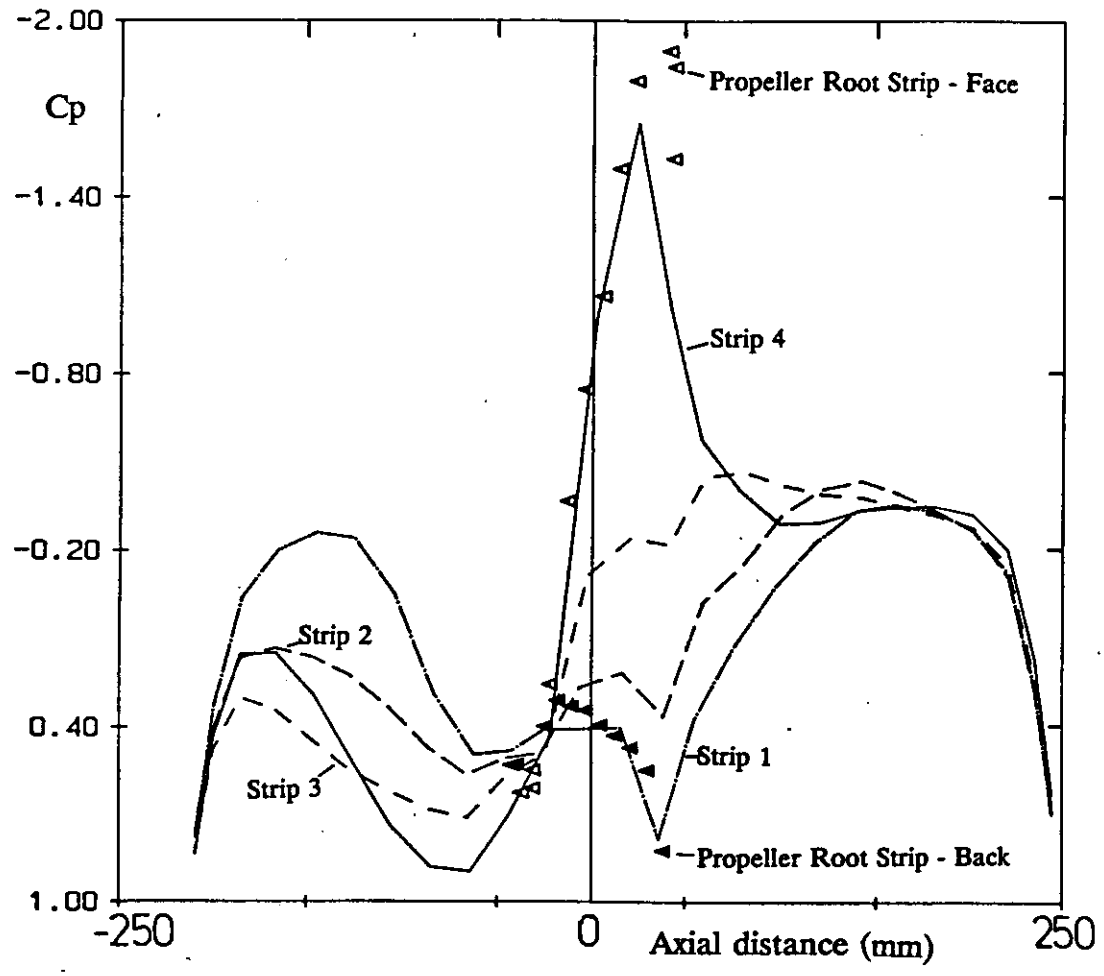

Figure 18 Pressure distribution on helical strips on propeller boss

shown in Figure 18. The values for the root strip of the blade are also plotted. A good match up between the blade root pressures is found with the adjacent hub strip. The discrepancy at the blade leading and trailing edge is probably due to the larger panel size on the boss. In the figure the difference in pressure downstream of the blade between adjacent strips 1 and 4 is due to the presence of the wake.

4.4 Velocity field downstream of propeller

In cylindrical coordinates, the fluid velocity induced by the propeller has three components. A component due to the axial acceleration, a radial component, and a circumferential or swirl component. The magnitude of each of these components is

dependent on the distance from the propeller plane of revolution, radial position and the angular position relative to the blade generator. For the four-bladed propeller used the velocity field repeats itself every 90^{o}.

The wake sheet downstream of the propeller determines the local structure of the velocity field. The discontinuity of potential across the wake sheet gives rise to large differences in the magnitude of velocity tangential to the panel surface. Also, the presence of the wake edge can lead to large local velocities. The determination of the velocity field downstream of the propeller is carried out on a regularly spaced grid of points. These points are evenly spaced in an axial, radial, and circumferential directions. Points generated in such a manner may coincide with the edge of a wake panel and cause a high local velocity. In a circumferential averaging process these points should be removed. A filtering criterion that the swirl velocity was not greater than 5 times the free-stream velocity was found to adequately smooth the velocity field. The spatial averaging of velocity at a given radius generates the time-averaged velocity for use as a rudder inflow velocity field.

Figure 19 shows a contour plot of lines of total disturbance velocity for a complete section through the propeller race at an advance ratio J=0.35 at 0.39 of a diameter downstream of the propeller. The position of the four blade generators are at 0^{o} , 90^{o}, 180^{o}, and 270^{o}. These values were obtained using a constant wake pitch (610mm) of constant diameter. The location of the wake sheet is seen as local regions of rapid change of velocity. This is especially marked at the inner and outer radial extent of the propeller blade (r=100mm and r=400mm).

In Figure 20, for the same conditions at a radius of 0.35D, the angular variation for the axial, radial and circumferential components of velocity are shown. The effect of the wake sheet discontinuity can be clearly seen. The justification for the filtering criterion is the rapid change in velocity through the wake sheet whereas for the rest of the cycle the changes are gradual.

The radial variation of the axial and circumferential (swirl) components of velocity

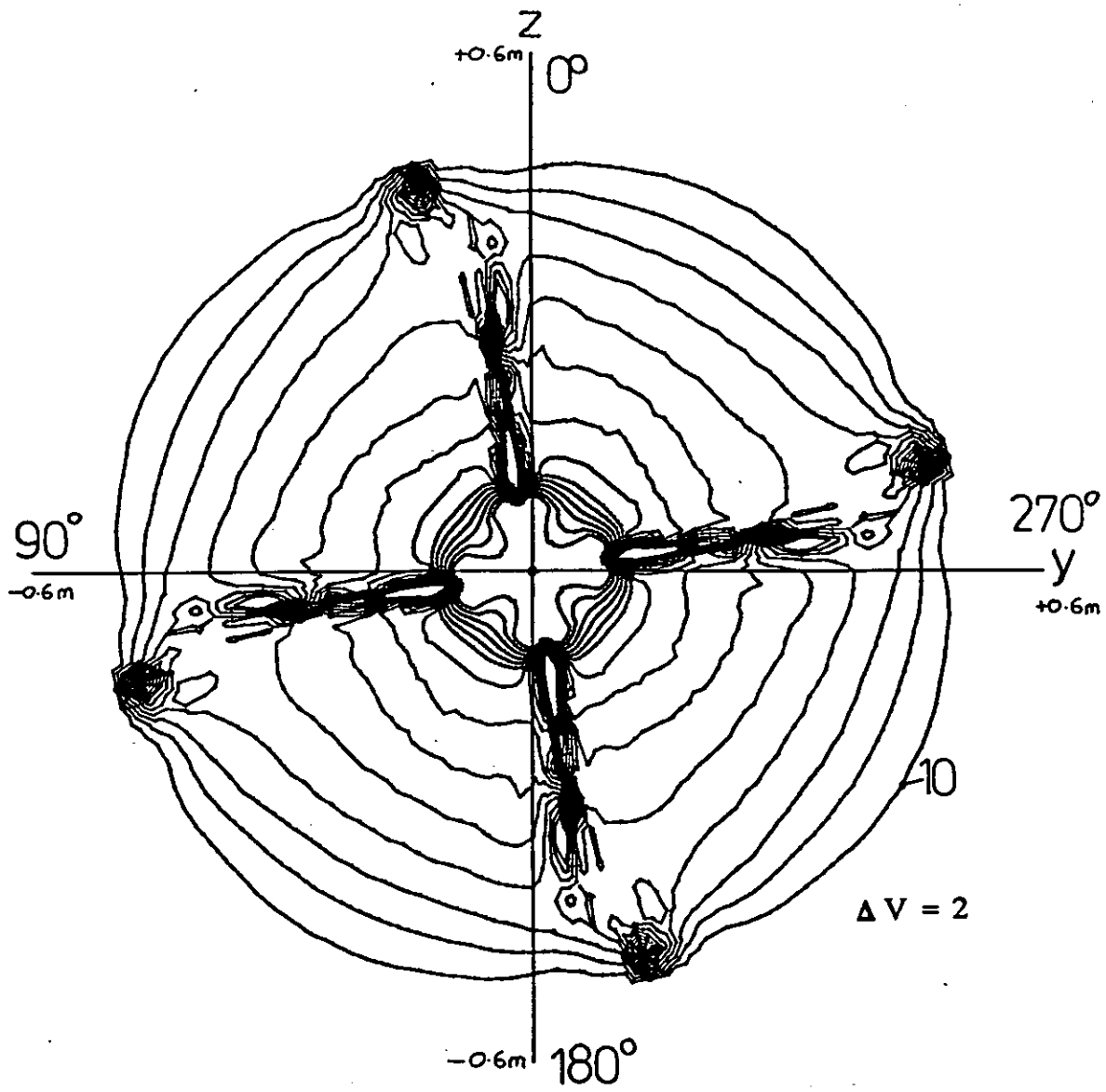

Figure 19 Contour plot of total velocity for vertical plane for J=0.35 at X/D=0.39 downstream of propeller

at X/D=0.39 is given in Figure 21 for both the fixed pitch wake (610mm) and the radially varying pitch geometry. Also, shown are the Blade Element Momentum results from Molland[8]. The fixed pitch wake gives a better comparison with the B.E.M. result. This is thought to be due to the distorted radially varying wake shape being ill-defined by the relatively low number of panels. Also, it should be noted that the B.E.M. results do not allow for the presence of the hub and that in this region the velocities are simply estimated.

The longitudinal variation in the circumferentially averaged velocity components for

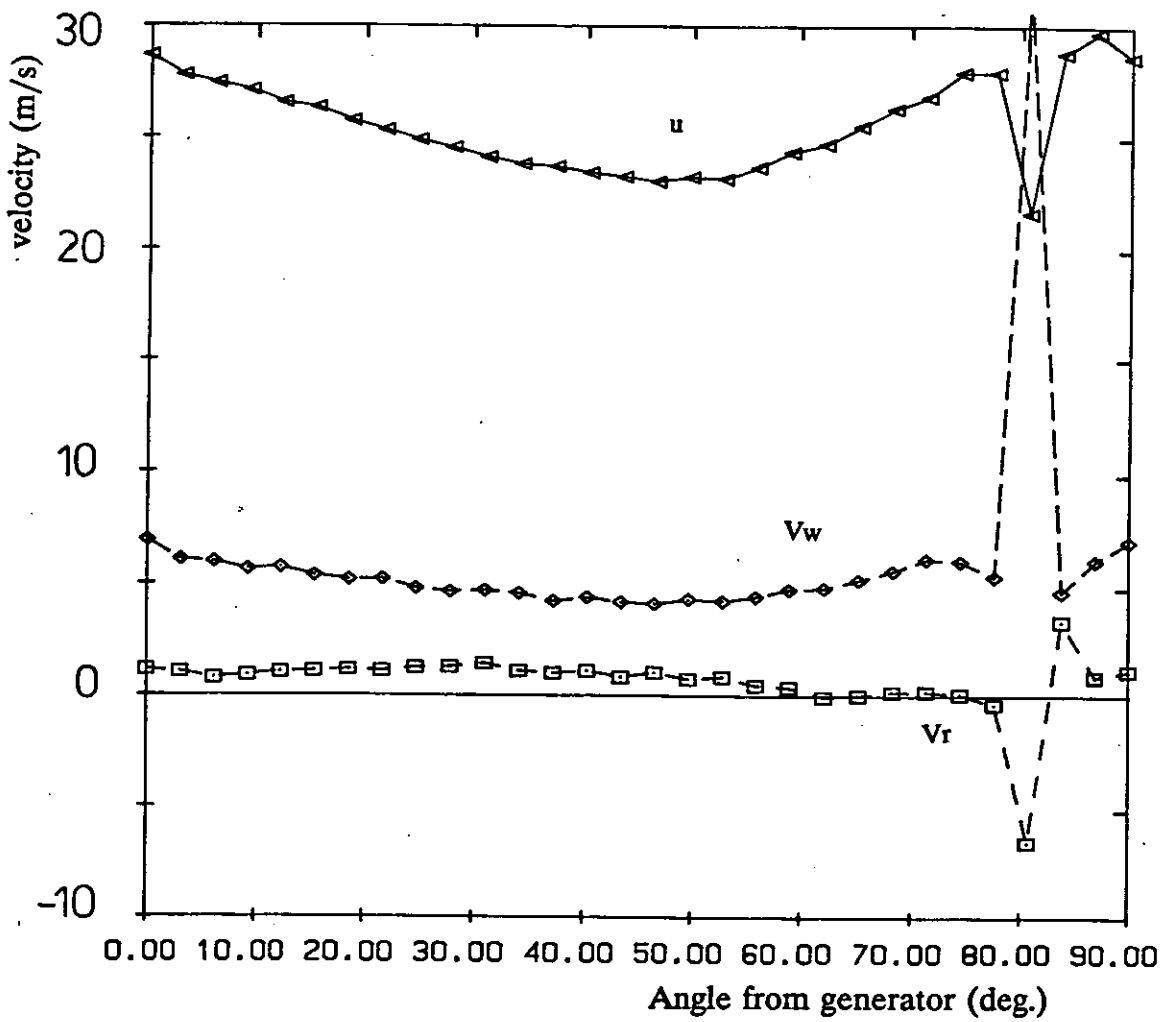

Figure 20 Circumferential variation of axial, radial and swirl velocity at X/D =0.39, r/D =0.35 and J=0.35

a radius of 0.35D is shown in Figure 22, as is the variation in velocity at the position y=0, z = 0.35D. The position where the wake sheet cuts the plane y=0 can be clearly seen. Overall, as expected from momentum theory the average velocity shows a slow increase with distance. The rapid acceleration of the flow occurs over the first 150mm from the propeller plane.

4.5 Summary

The 400 panel blade and boss model of the modified Wageningen B4.40 propeller with a fixed pitch wake geometry based on Blade-Element Momentum theory gives a

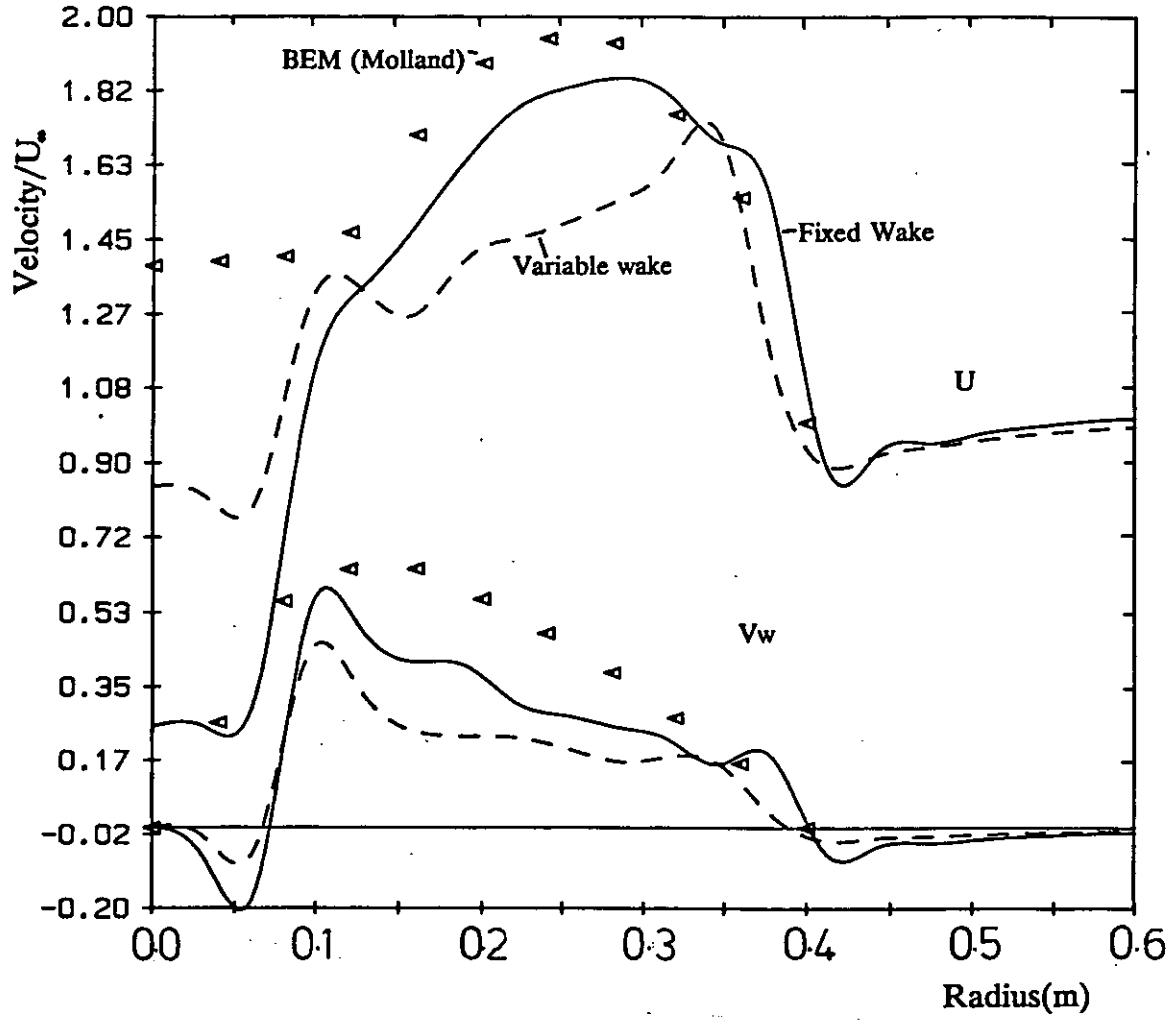

Figure 21 Radial variation of axial and swirl velocity at J=0.35 and X/D=0.39

reasonable representation of propeller characteristics for the purposes of considering rudder-propeller interaction. The over-prediction by 10% is of the same order as that found for the rudder model. It is considered that the propeller blade loading and the resultant downstream velocity field is representative of that due to the actual blade loading.

The crude representation of the wake is acceptable at present, although future work should allow a more sophisticated representation to be developed. It is hoped that time accurate LDA measurements will aid in the development. In the absence of such information for validation it was decided that as simple as possible a model would at least allow a consistent approach to be used for all advance ratios.

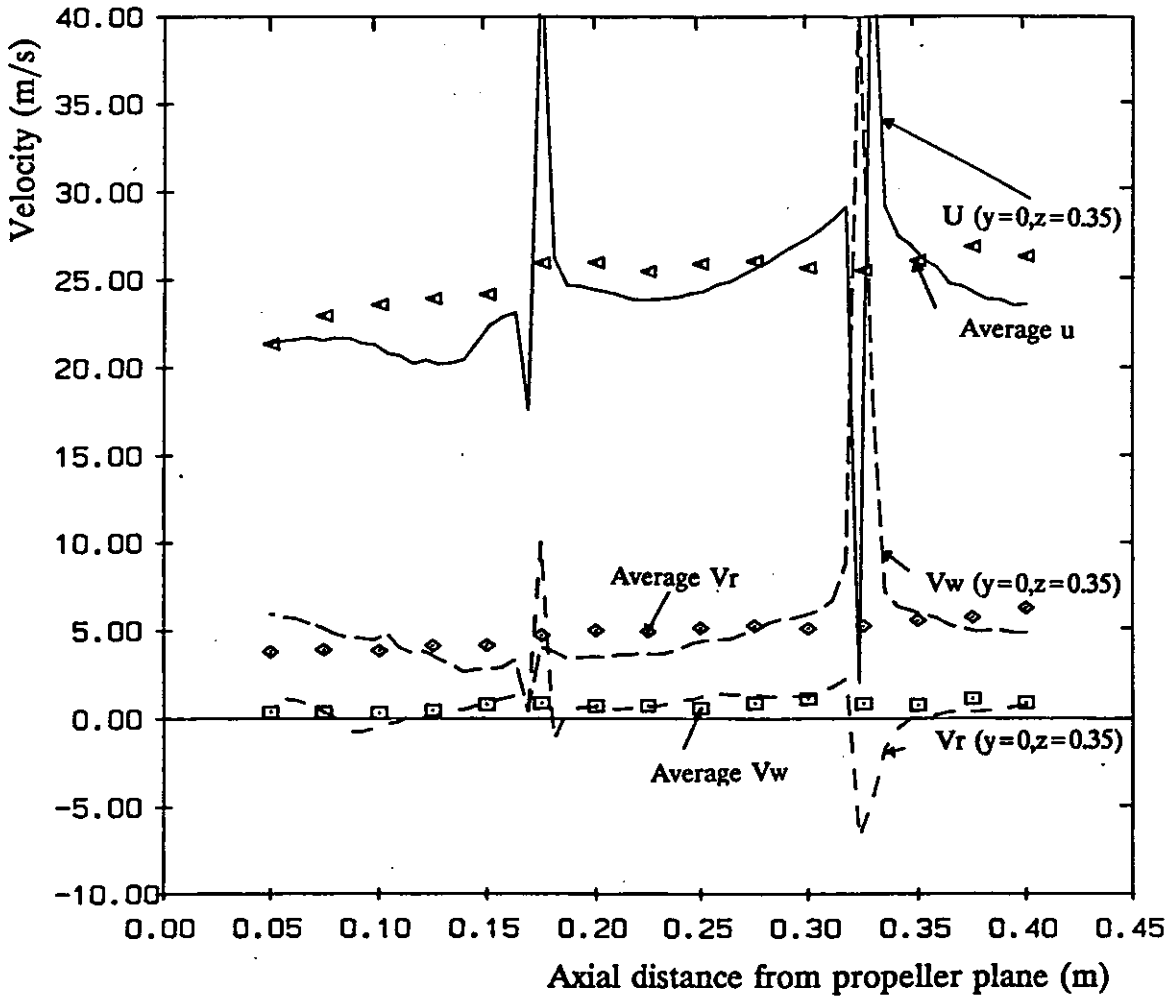

Figure 22 Longitudinal variation of axial, radial and swirl velocity at J=0.35

The velocity field downstream of the propeller, for the purposes of modelling the interaction, can be found by inspecting 30 points per radius. A filtering process was used to remove spurious wake panel edge velocities. Overall, the fixed pitch wake appeared to give a better representation of the velocity field than the variable pitch model.

5 INTERACTION OF RUDDER AND PROPELLER

5.1 Introduction

The method chosen to model this interaction is to separate the rudder and propeller

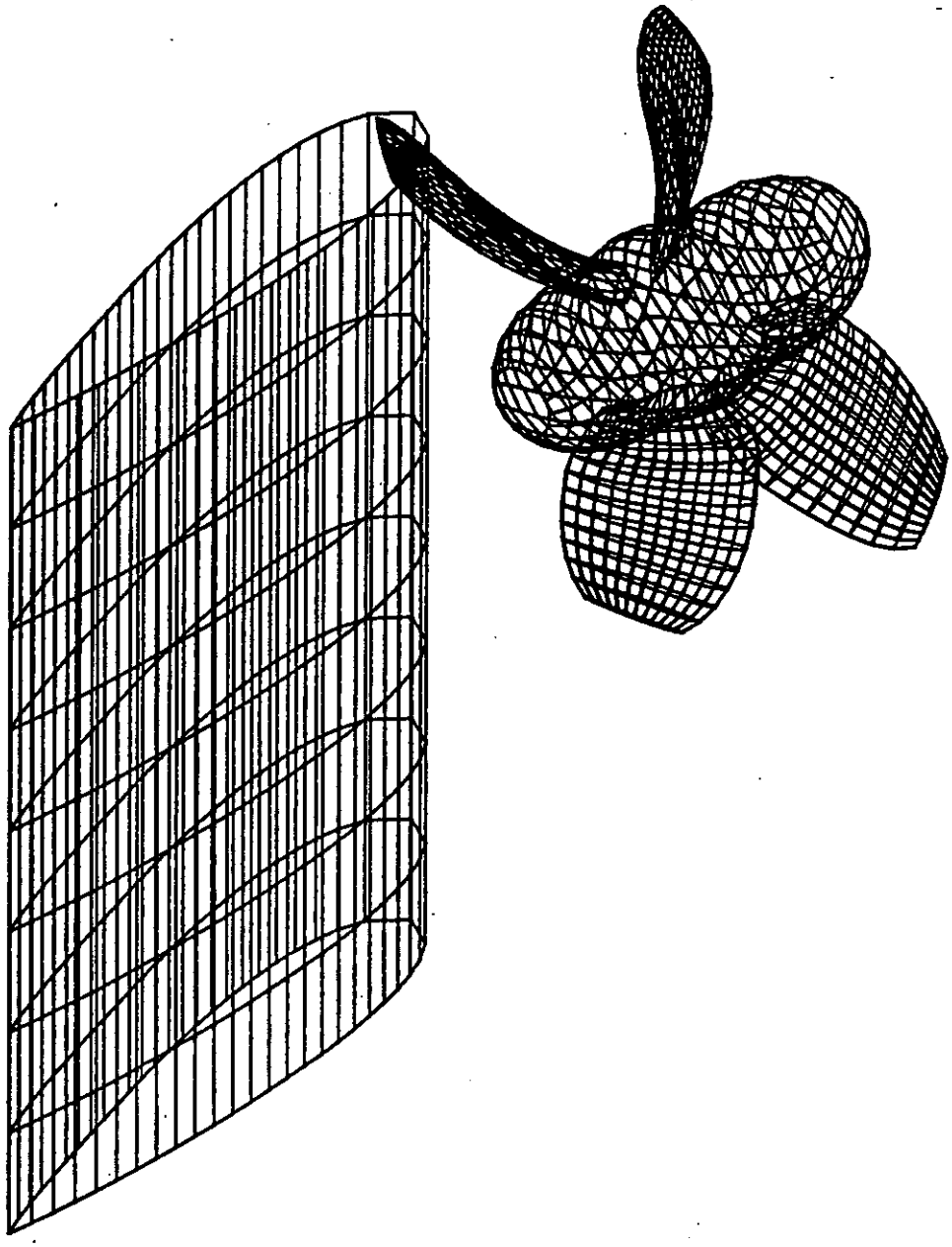

Figure 23 Isometric wire-frame view of the relative position of rudder and propeller for validation exercise

and account for the interaction between them through the use of a modified inflow. The previous two sections have covered the application of a surface panel method to the analysis of a free-stream rudder and free-stream propeller. This section details how the interaction velocity field is applied to the separate models to account for their mutual influence.

To verify the interaction velocity field method a particular geometry is considered in detail. This case is that of the mid-longitudinal separation X/D=0.39 at the three

experimental test advance ratios of 0.35, 0.51, and 0.94.

5.2 Geometry

The relative position of rudder and propeller model is shown in Figure 23. It should be noted that this is not how the flow is modelled. The rudder and propeller are separately modelled with their mutual influence accounted for by modification to their respective inflows. The numerical models used are identical to those described in the previous two sections. The propeller axis is 600mm above the tunnel floor. There is no lateral separation and the longitudinal separation of propeller plane and rudder stock is 512mm. The maximum height of the propeller blade is coincident with the tip of the rudder.

5.3 Interaction Velocity Field Algorithm

The development of the PALISUPAN software, as a series of procedures corresponding to the various stages in solving the perturbation potential method, allowed a specific program to solve rudder-propeller interaction to be written. Figure 24 is a flow chart of the overall process. The format of the geometry input file allowed the information defining both the rudder and propeller to be held in store on the host transputer without the need to re-load from file for each iteration cycle.

First the propeller geometry is loaded across the network and the panels generated. The propeller is solved first due to the stronger influence of the propeller on the rudder. The circumferential averaged velocity field at the rudder stock position is found and the rudder inflow velocity field modified accordingly. The rudder geometry is then loaded across the network, panels generated, and the flow about it solved. A circumferentially averaged propeller inflow velocity field at the propeller plane is found and the whole cycle repeated until convergence is deemed to have occurred. Relevant information is filed after each flow solution and velocity field generation. The program structure allows the flow to be solved for a series of rudder incidence.

5.4 Rudder Interaction Velocity Field

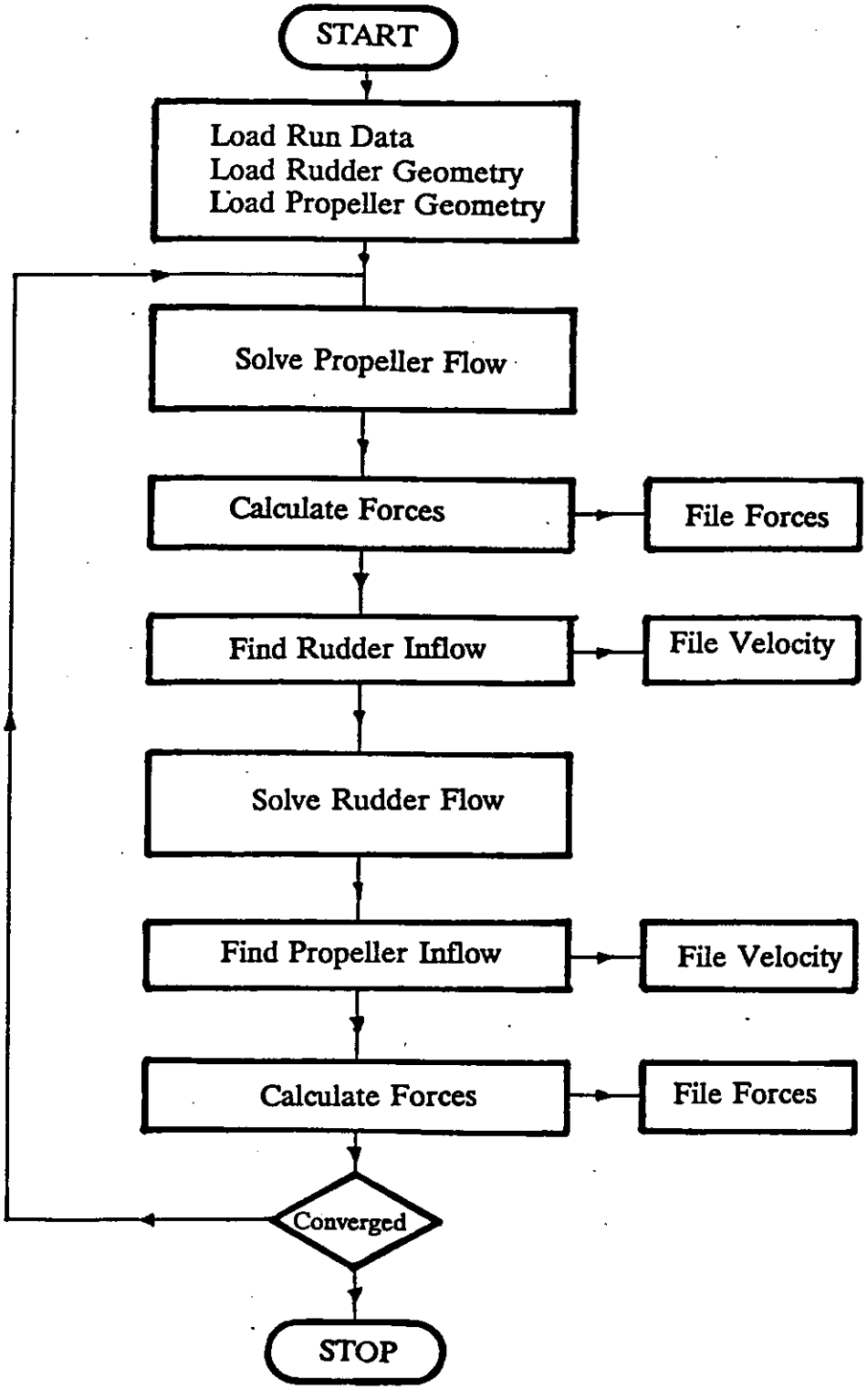

Figure 24 Flow chart of Interaction Velocity Field Algorithm

The interaction velocity field downstream of the propeller at the rudder position is generated as described in the previous section. A circumferential average value for a given radial position is found with the filtering out of large velocity discrepancies. If an axially varying inflow field is to be used, this process is repeated at a regular axial spacing to give a series of time averaged velocities. At each axial station the rudder inflow velocity is the vector sum of the free-stream velocity and that due to the propeller interaction. The three components of velocity (axial U, radial Vr, and swirl Vw) are specified at a regular series of radially spaced points relative to the origin of the propeller axis (xo,yo,zo). The inflow velocity field store uses this information to specify the cartesian components of velocity for a given spatial location (x,y,z) in the following manner:

$$U(x, y, z) = U_0 + U(x)\, a + Vr(x)\, r + Vw(x)\, w$$

$$\text{where} \quad a = (1, 0, 0)$$

$$r = (0, (y - yo), (z - zo)) \qquad [4]$$

$$\text{and } w = a \times r$$

The data defining the initial velocity field is included in the geometry input file. At subsequent iterations the velocity field calculation process modifies the values stored on the Host prior to the generate panel phase. An inflow velocity defined at 20 radial stations with averaging over 30 points per radius was found to be acceptable.

5.5 Propeller Inflow Velocity Field

A spatially averaged velocity field at points in a cylindrical tube upstream of the rudder is obtained. This allows the average reduction in axial velocity passing through the propeller due to the rudder to be found. Also, spatially averaged swirl, and radial components can be found. The velocity field including the inflow velocity is generated on a cylindrical disk for inclusion in the geometry input file in an identical manner to that for the rudder. The velocity field at 10 radial points averaged over 20 points at 18^{o} increments was found to adequately define the propeller inflow.

5.6 Iteration and Convergence

The downstream position of the rudder means the propeller has a far greater influence on the rudder than the rudder has on the propeller. Therefore, the first stage in determining the interaction is to solve the flow around a free-stream propeller, then generate the propeller's downstream velocity field and apply to the rudder. On solution of the rudder flow the rudder upstream velocity field is obtained. This field is then applied to the propeller and the process is repeated until convergence has occurred.

A number of convergence criteria are possible. The application of the work is for manoeuvring characteristics in which of prime interest is the rudder sideforce. Therefore, the convergence of total rudder lift was chosen.

For the representative geometry at a rudder incidence of -0.4^{o} and $J=0.35$ the convergence behaviour of both the propeller and rudder forces were investigated. Figure 25 plots the percentage variation in rudder side-force C_L with each complete iteration cycle (for the first cycle the difference is between the free-stream value and the interaction result). The realtive change in C_L is plotted using a $\log_{10}$ scale. It can be seen that convergence is rapid. Similar behaviour was found at the other advance ratio and for different rudder incidence. The other components of rudder and propeller forces exhibited a similar rapid convergence. For this work a 0.5% variation in rudder sideforce was deemed to be an acceptable convergence criterion. In general, 2 or 3 iteration cycles were required for convergence.

For the parametric studies of Chapter 8 the final rudder inflow velocity field at zero incidence was used for all rudder incidence as the variation in sideforce due to the interaction was unlikely to alter the trends of the results as the performance was modelled for incidence close to zero ($< 10^{o}$) where the velocity field does not change significantly.

5.7 Comparison of model and experiment

The numerical model results presented are for a series of rudder incidence corresponding to the values used in the experimental tests of -30.4^{o}, -20.4^{o}, -10.4^{o}, -0.4^{o},

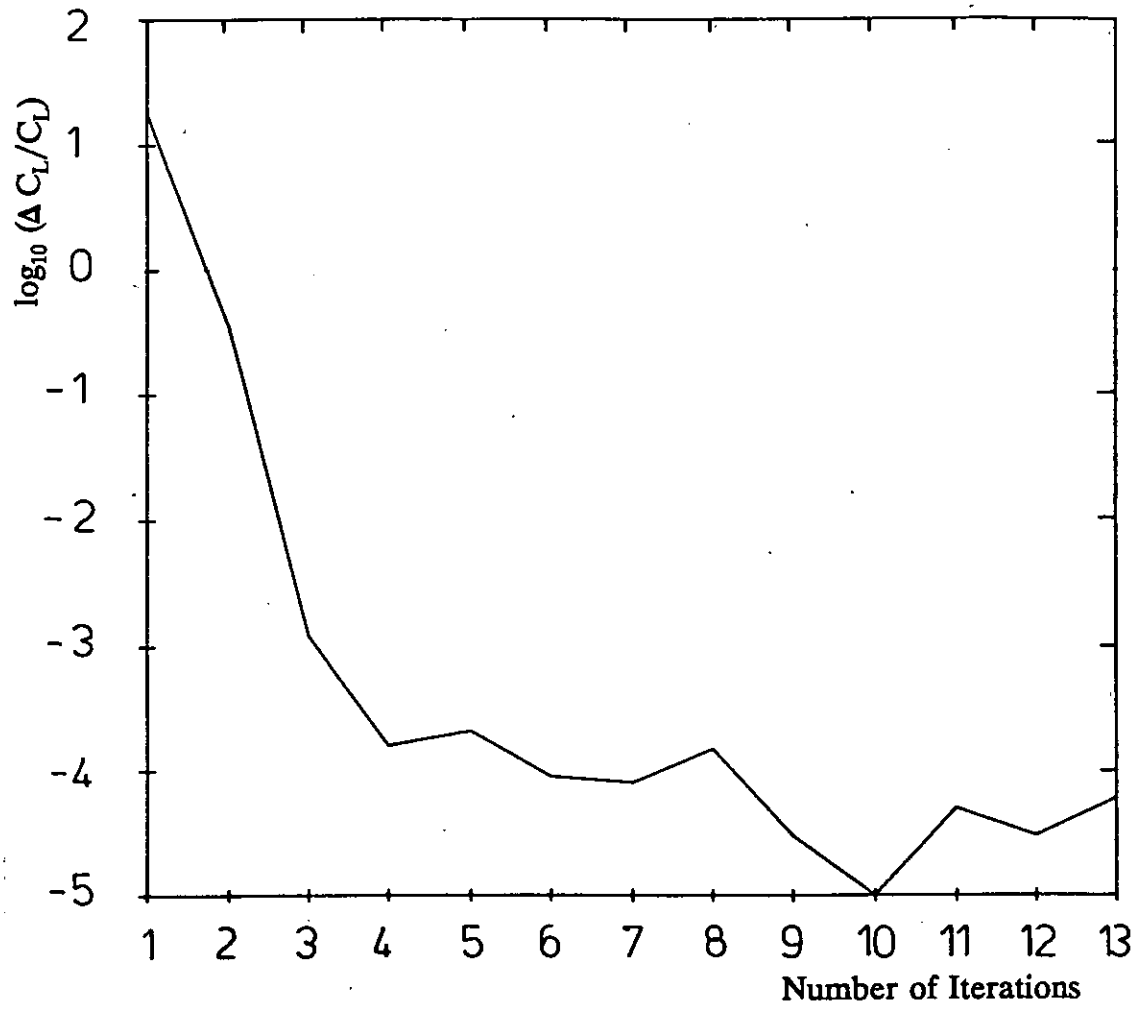

Figure 25 Convergence of rudder lift with number of iteration cycles

9.6^{o}, 19.6^{o}, and 29.6^{o}. The experimental test advance ratios were used with a detailed comparison for an advance ratio of 0.51.

A series of sensitivity tests were carried out at J = 0.51 for a rudder incidence of $+9.6^{o}$. The results for this condition were representative of the behaviour at other incidence and advance ratio. The convergence behaviour of rudder C_L and C_D with panel density was similar to that for the free-stream rudder. To investigate the satisfactory capture of the flow physics, figures for the spanwise variation of sectional lift coefficient will be shown.

The variation of the spanwise loading with increased number of chordwise and

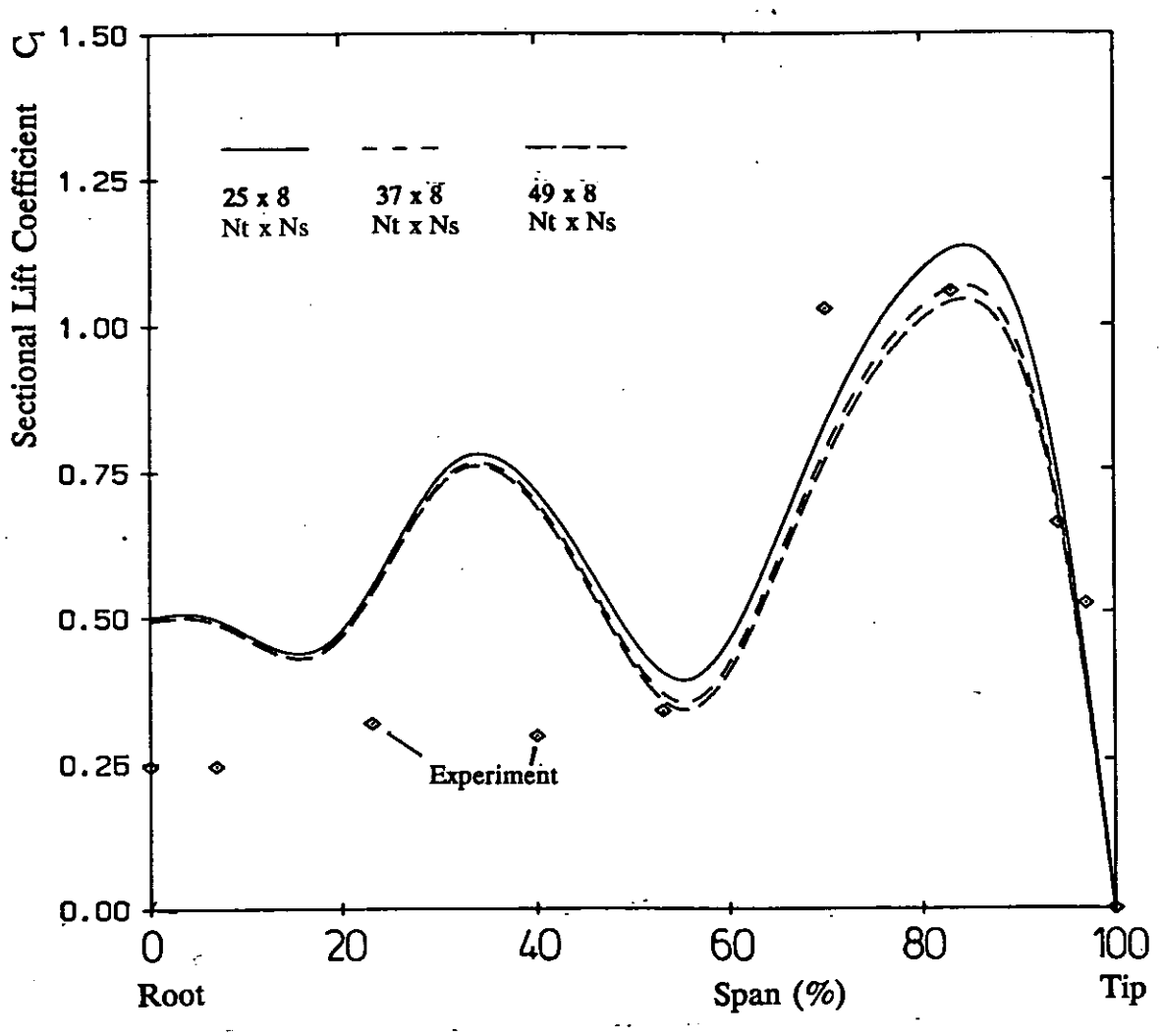

Figure 26 Variation of spanwise loading: Effect of the number of chordwise panels for Rudder No. 2 at J=0.51 and $+9.6^{o}$

spanwise panels is shown in Figures 26 and 27 respectively. In a manner similar to the propeller blade the shape is more sensitive to the number of spanwise panels. Therefore, a panel distribution with Nt = 25 and Ns =16 was used for all subsequent cases. Regular panel spacing was used in the spanwise direction and sinusoidal clustering at the leading and trailing edges in the chordwise direction.

The effect of the more regular velocity field generated by a fixed pitch wake is clearly seen in Figure 28, the radially varying wake velocity field results in a smearing out of the spanwise load distribution. Therefore, the fixed pitch wake was used for subsequent tests.

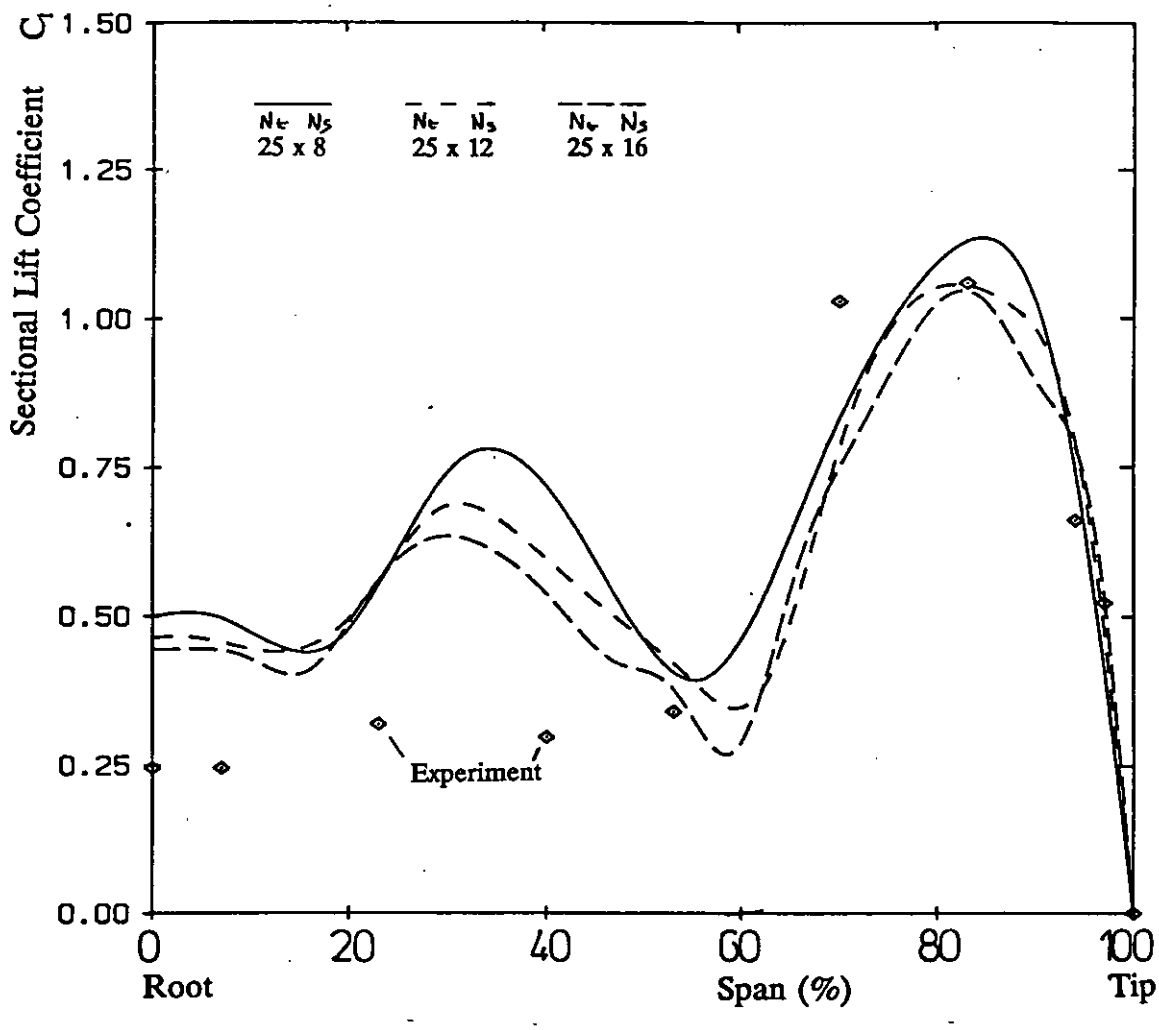

Figure 27 Variation of spanwise loading: Effect of the number of spanwise panels for Rudder No. 2 at J=0.51 and $+9.6^{o}$

The previous comparisons were for a rudder inflow velocity field generated at the position of the rudder leading edge. The effect of longitudinal variation in the axial position used to generate the velocity field is shown in Figure 29 for velocity fields generated at the rudder leading edge, rudder stock and trailing edge. It is likely that the velocity field at the stock is the most representative average velocity value; the value will be weighted toward the leading edge as this is the most sensitive region for rudder loading. Therefore, the velocity field used for subsequent tests is located at the rudder stock.

In the previous figures the numerical result under-predicts values at the tipwise hump

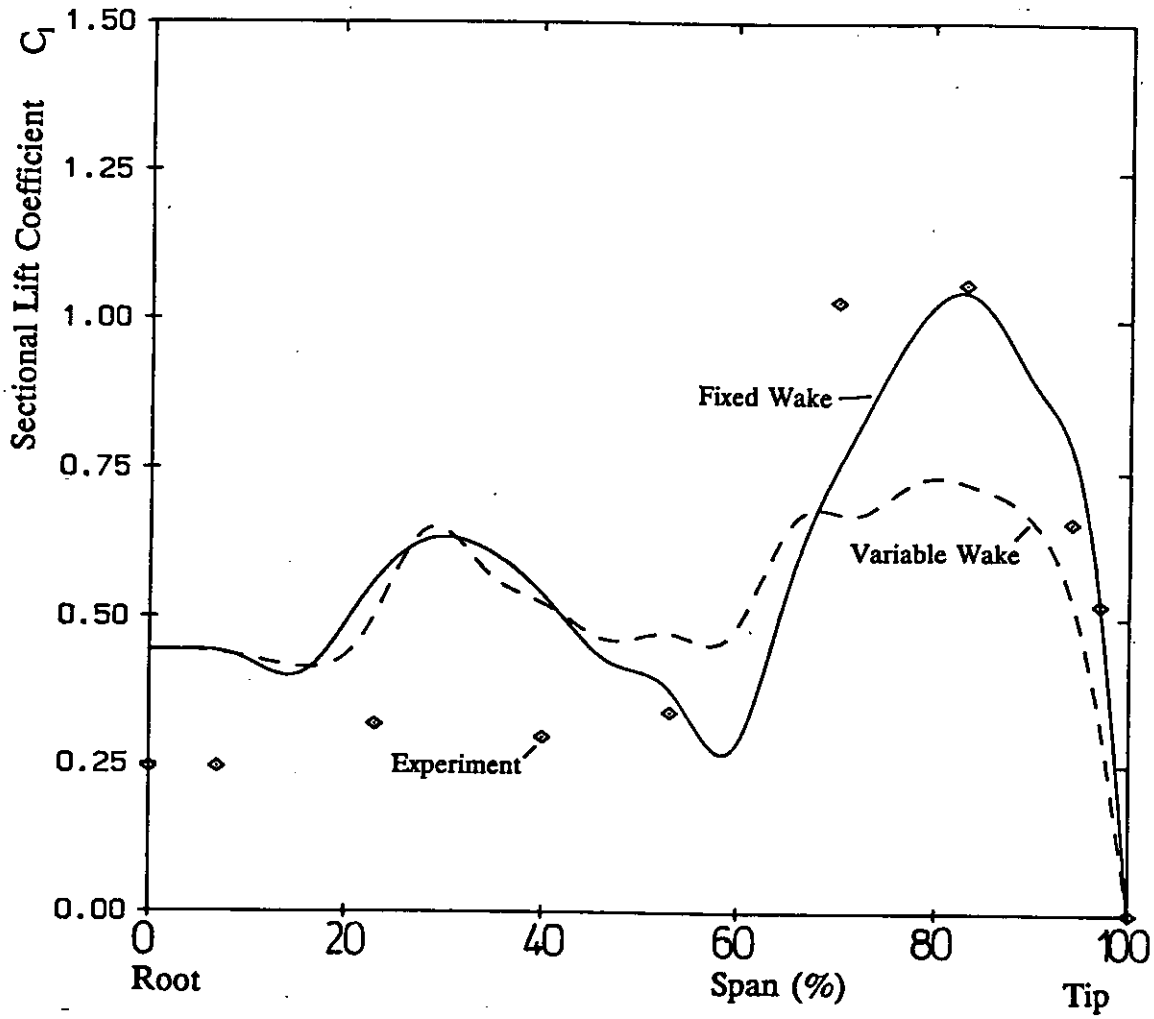

Figure 28 Variation of spanwise loading: Effect of the propeller wake model for Rudder No. 2 at J=0.51 and $+9.6^{o}$

(80% span) and over-predicts those at the inner hump (30% span). A similar result was found by Molland [4] using lifting-line theory. Both the inner and outer hump require extra experimental points to satisfactorily resolve the actual shape. However, it appears some of the flow physics is ignored. To attempt to resolve this the following were considered:

1) Figure 30 compares results for B.E.M. result of Molland[8] for the velocity field downstream of the propeller (see Fig. 7.20) and for a rudder inflow with a 20% increase in the inflow angle, defined thus θ:

with a constant total velocity at a given radius but with energy redistributed from the axial

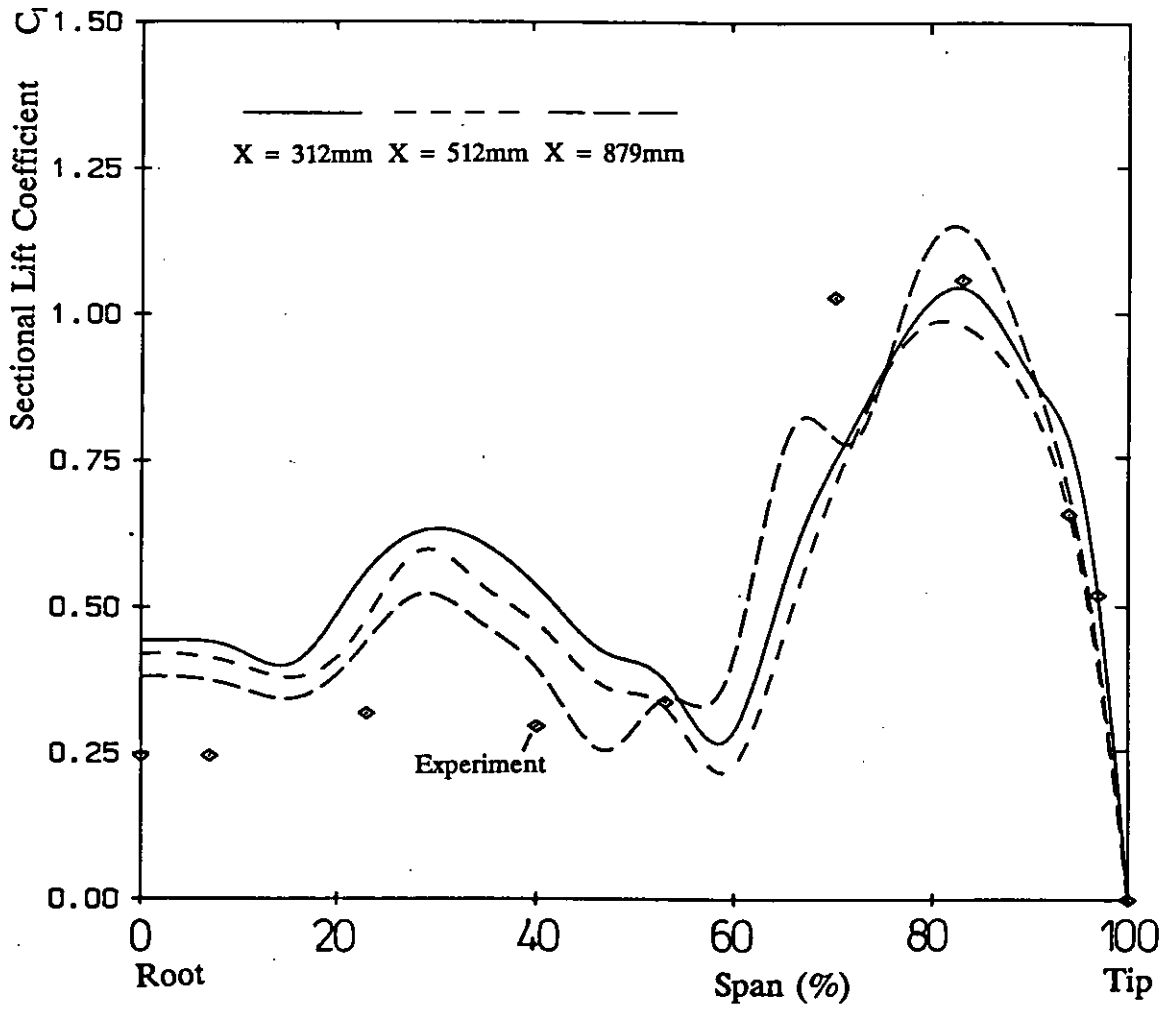

Figure 29 Variation of spanwise loading: Effect of the longitudinal position of velocity field for Rudder No. 2 at J=0.51 and $+9.6^{o}$

$$V_T = \sqrt{U^2 + Vw^2} \quad where\ \theta = \tan^{-1}\left[\frac{Vw}{U}\right]$$

$$for\ \theta' = 1.2\ \theta \qquad [5]$$

$$U' = V_T \cos\theta' \quad and \quad Vw' = V_T \sin\theta'$$

to the swirl direction. This attempts to see how sensitive the result was to the distribution of axial and swirl velocity within the race. The B.E.M. result over-predicts the 80% hump while reducing the 30% hump excess. The 20% increase in θ does not affect the 80% hump while it does reduce the 30% hump. It was decided to not modify through the use of the empirical data to obtain a better fit as the modification would only have limited application.

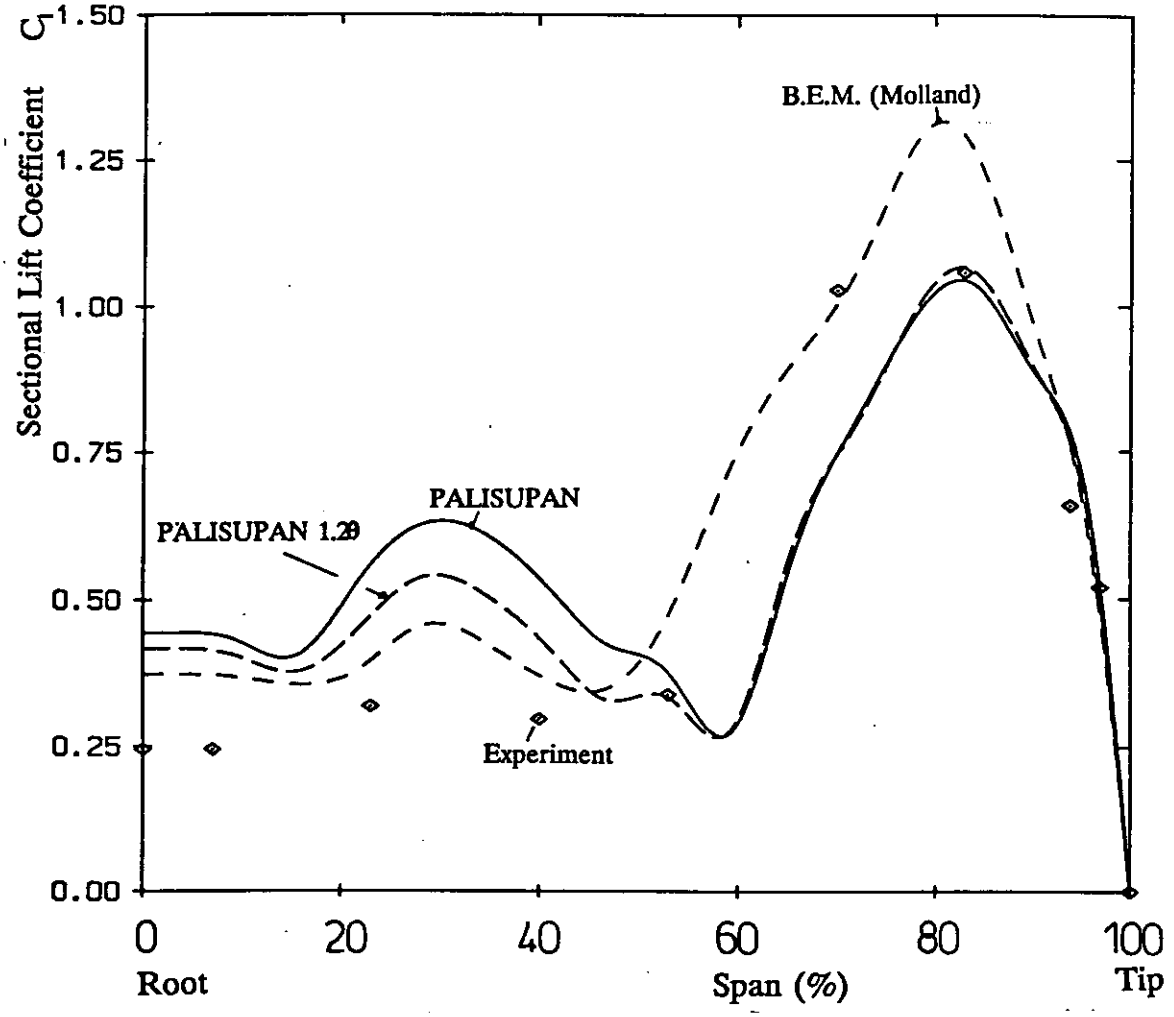

Figure 30 Variation of spanwise loading: Effect of modifying velocity field for Rudder No. 2 at J=0.51 and $+9.6^{o}$

2) In Figure 31 the effect of gap between the rudder root and wind tunnel floor was investigated. In the experimental tests this gap was 5mm although there was some flow through the hole through which the rudder stock passed to the dynamometer which could potentially lead to a greater gap effect. It can be seen that the non-physical 50mm and 100mm gaps are effective at reducing the 30% hump and match the root region lift. However, the 5mm gap, as expected, only has a minimal effect. As it is physically realistic it was retained in the model by setting the reflection plane at
z= -5mm.

3) The effect of the turbulent boundary layer flow along the wind tunnel floor was

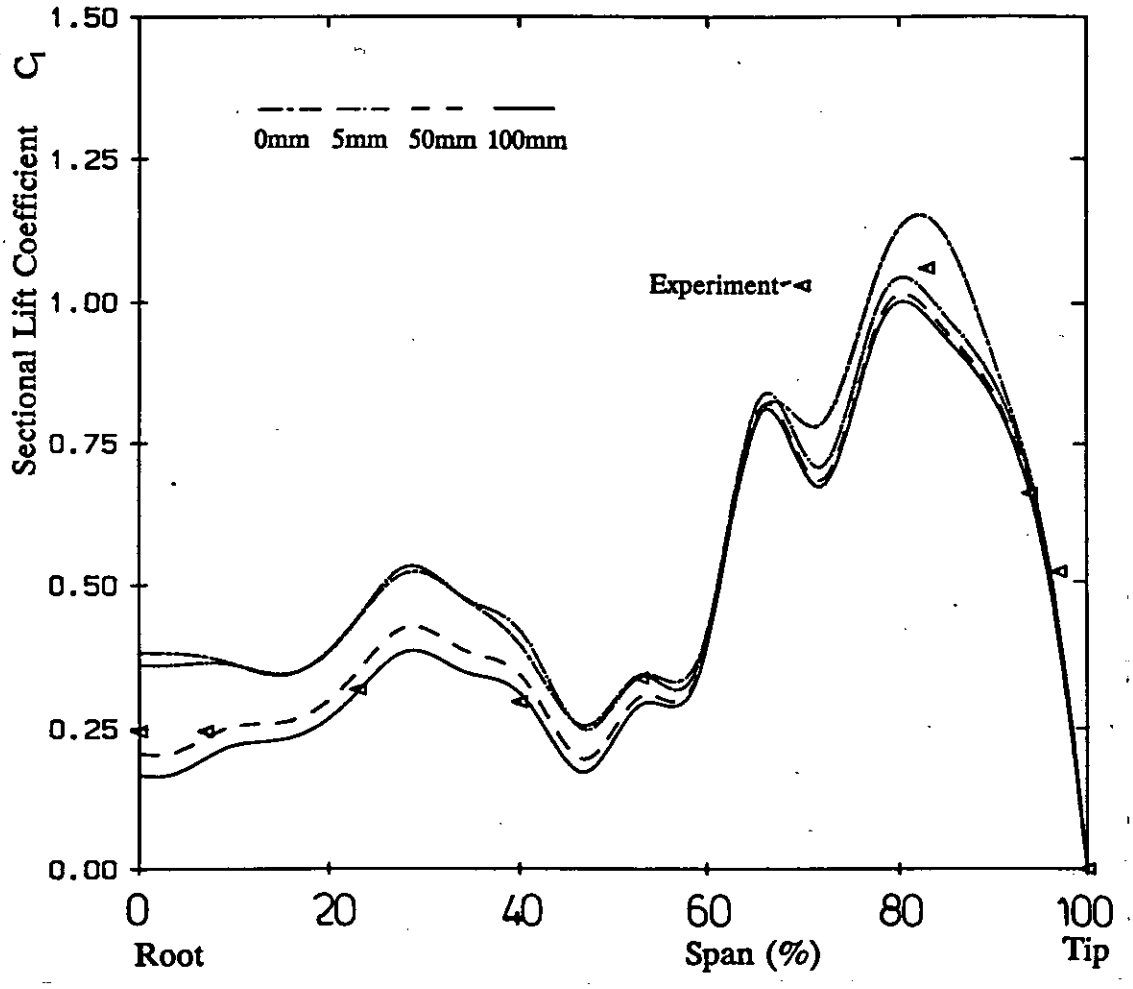

Figure 31 Variation of spanwise loading: Effect of rudder root gap for Rudder No. 2 at J=0.51 and $+9.6^{o}$

investigated by reducing the axial velocity in the boundary layer. The standard relationship for turbulent boundary layer development with an assumed $1/7^{th}$ power velocity variation with height was used. Figure 32 shows the effect of two assumed boundary layer thicknesses of 91 and 126mm corresponding to the realistic boundary layer development length at the rudder of 5m and a value double that of 10m. These both appear to model the root region well. The 5m long turbulent boundary layer correction to the inflow velocity field was therefore retained . However, there is little effect on the load distribution in way of the propeller.

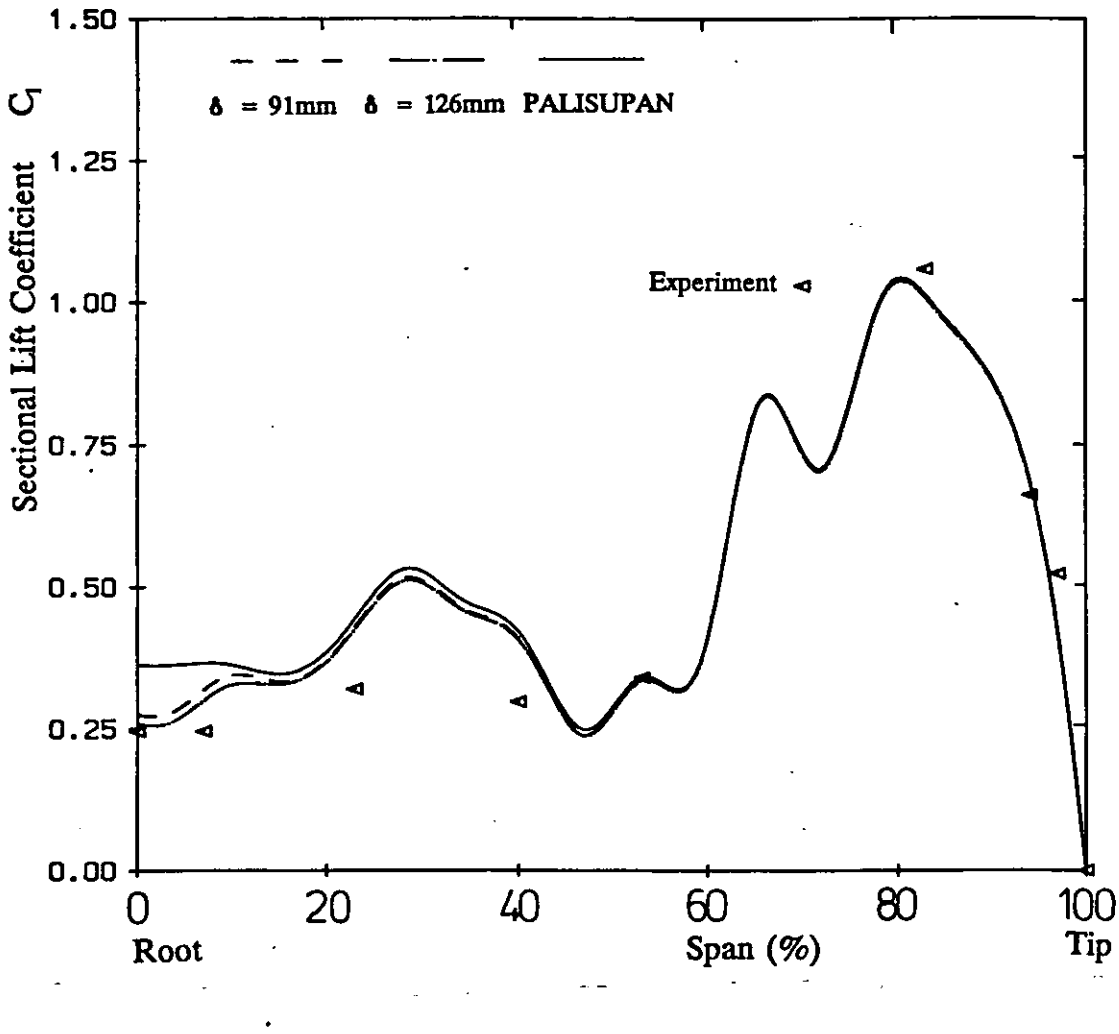

Figure 32 Variation of spanwise loading: Effect of tunnel boundary layer for Rudder No. 2 at J=0.51 and $+9.6^{o}$

Remaining physical reasons for this disparity between experiment and theory are potentially the tip vortex holding up the outer hump although this effect is included in the lifting-line model and does not appear to affect the 30% hump. More probable contenders are the quasi-steady assumption, especially for the propeller. If each blade was modelled with the actual cross-flow induced by the rudder there might be an alteration of the propeller race direction away from the propeller axis. The direction of this alteration would depend on the sign of the rudder incidence and be symmetric about $\alpha = 0^{o}$. A similar effect could occur due to the presence of the ground board inducing a cross-flow due to the highly rotational propeller wake and its image. Such an effect would be likely to depend mainly on the direction of rotation and thrust of the propeller and be non-symmetric about $\alpha=0^{o}$.

Although the predicted spanwise load distribution does not exactly follow that measured, the correspondence was considered sufficiently close that the Interaction velocity Field method was considered acceptable for modelling rudder-propeller interaction for the purposes of predicting manoeuvring performance and for parametric design studies.

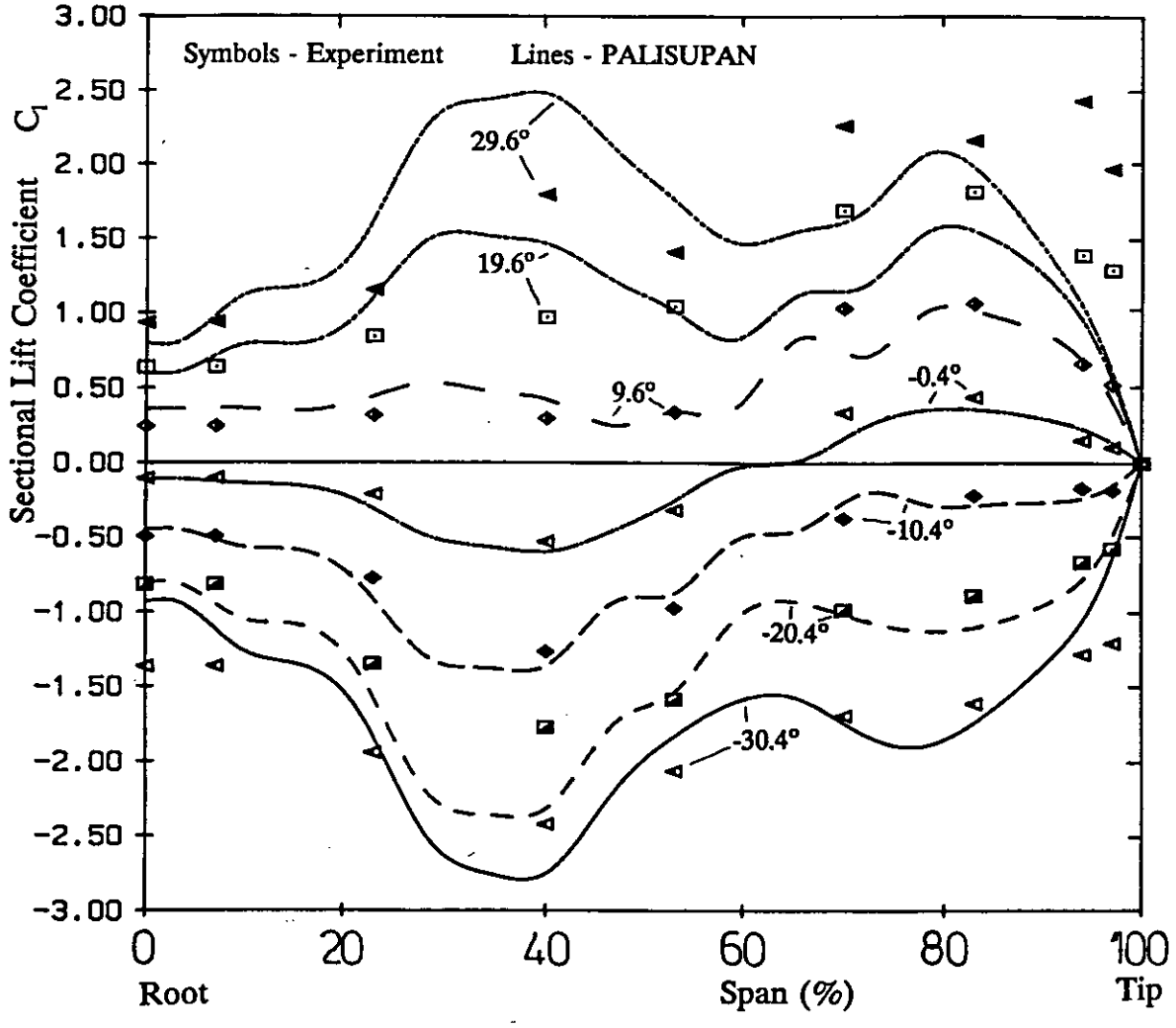

Figure 33 Comparison of lifting-surface and experimental spanwise load distribution for Rudder No. 2 at J=0.51

In Figure 33, the numerical and experimental results are compared for seven angles between -30.4^{o} and +29.6^{o}. The comparison between -10.4^{o} and +9.6^{o} is good. The shape gradually distorts away as the magnitude of incidence increases further. For positive incidence the 30% hump is over-predicted and the 80% hump under-predicted. For negative incidence, the 30% hump is overpredicted and the 80% hump fairly well modelled although as with the free-stream comparison the clear tip vortex effect is not modelled. The symmetry of behaviour with incidence suggest the effect most likely to account for the difference in spanwise loading is likely to be due to the rudder induced cross-flow at the propeller.

In Figure 34 the actual and predicted quasi-steady pressures are compared for three advance ratios at α = -0.4^{o}. The overall shape and values compare well apart from the 53% and 70% span positions. The experimental shape at 53% is unusual and is likely to be strongly affected by viscous/separation effects in the shadow of the hub. The predicted hub region/blade root velocity flow obviously does not reproduce this although the value of sectional lift (see Fig 7.32) is found. The high value of leading edge load at 70% span indicates the predicted velocity field just outside the hub region is underpredicted and reflects on the crude representation of the propeller wake.

Finally, for Rudder No. 2, Figure 35 presents the force characteristics comparison for three advance ratios. For rudder lift the variation both with incidence and advance ratio is very good. This is true even up to 30^{o} incidence for J=0.35 and J=0.51. This is considered to be due to the hysteresis effect induced by the cyclical variation of flow preventing stall and thereby maintaining potential flow to higher incidence. Although the exact load distribution is not predicted the total appears a reasonable representation. It is noted that the total energy of the propeller race which helps generate the lift is predicted well and so although the energy distribution within the race is not correct the overall induced load is.

The drag prediction is reasonable at low incidence but at higher incidence ($>10^{o}$) only gives about 70% of the experimental value. This is due to the viscous force estimate not correctly representing the complex boundary layer flow. A similar behaviour was seen for the free-stream rudder performance.

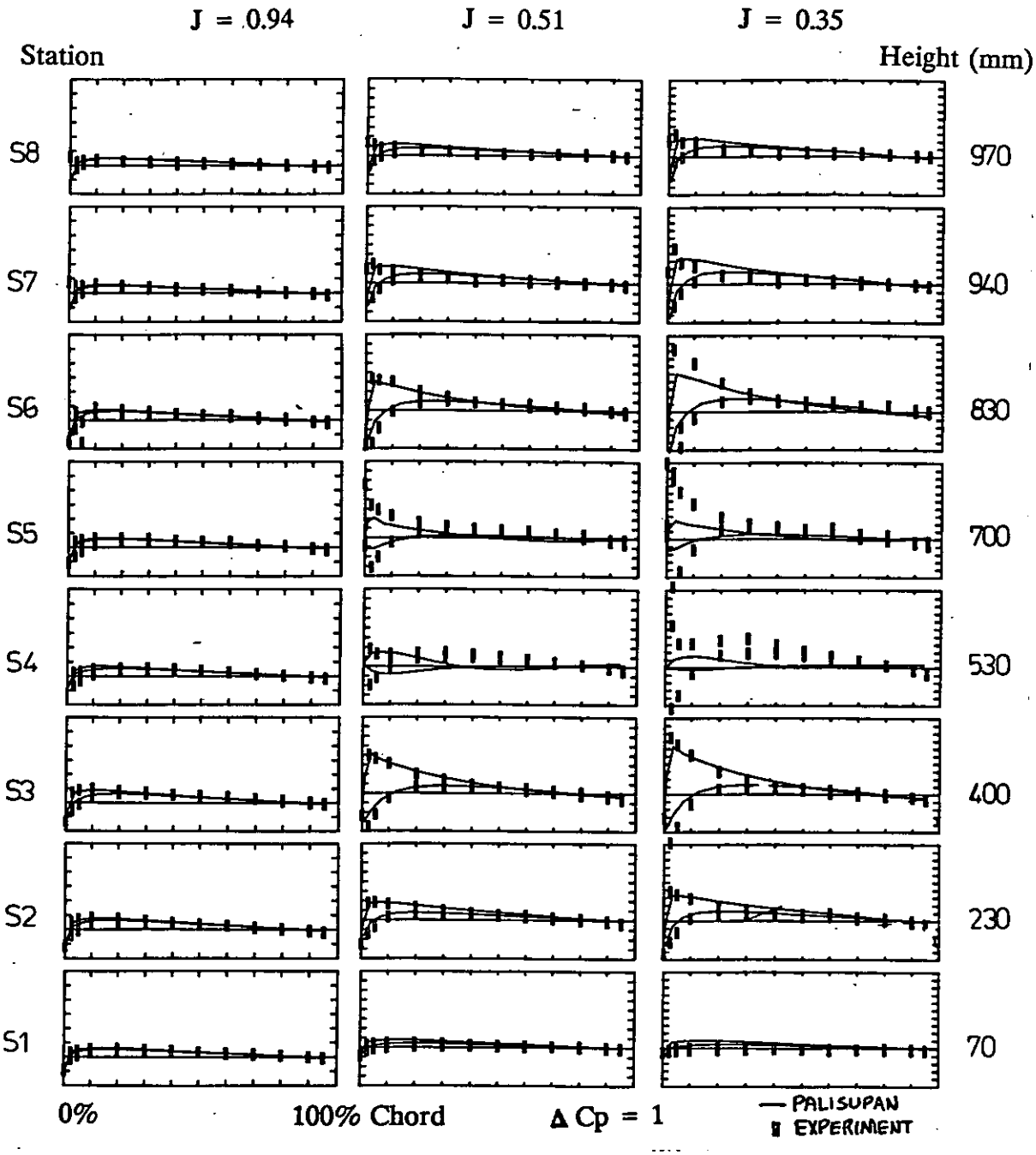

Figure 34 Comparison of lifting surface and experimental pressure distributions for Rudder No. 2 at J= 0.94, 0.51 and 0.35

The chordwise position of centre of pressure is within 5% of the experimental value between $-20^{o} < \alpha < +20^{o}$ with a better prediction at J=0.35. The deviation for greater incidence is due to the viscous flow/stall effects altering the shape of the pressure distribution and hence CMz and CPc.

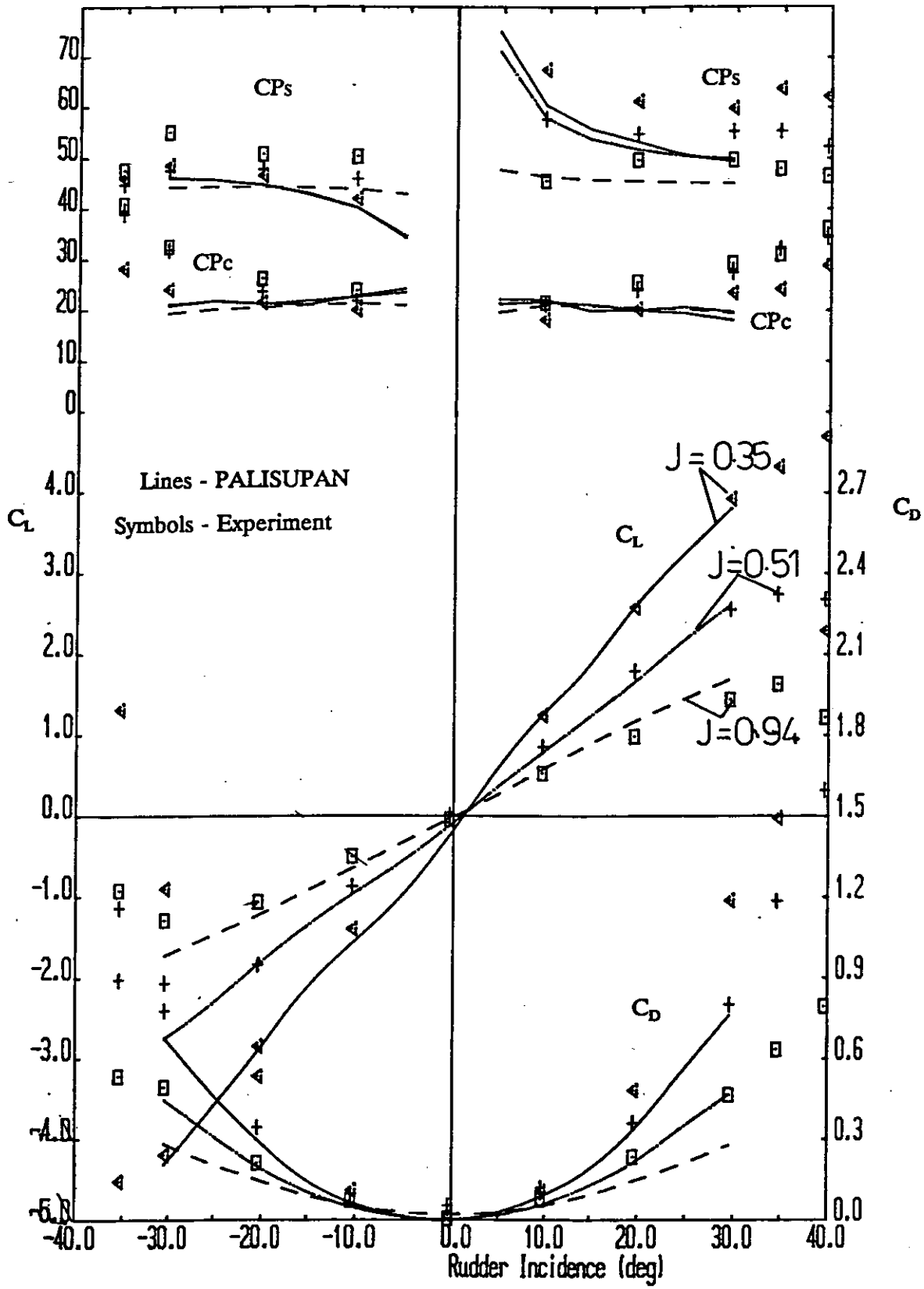

Figure 35 Comparison of lifting surface and experimental Rudder No. 2 force characteristics for J =0.94, 0.51 and 0.35.

The spanwise position of the centre of pressure is within 5 to 10%. It is likely the tip vortex has a strong effect especially at high incidence. The movement with change in J is identified by the numerical model.

The effect of the rudder on propeller thrust at different rudder incidence is shown in

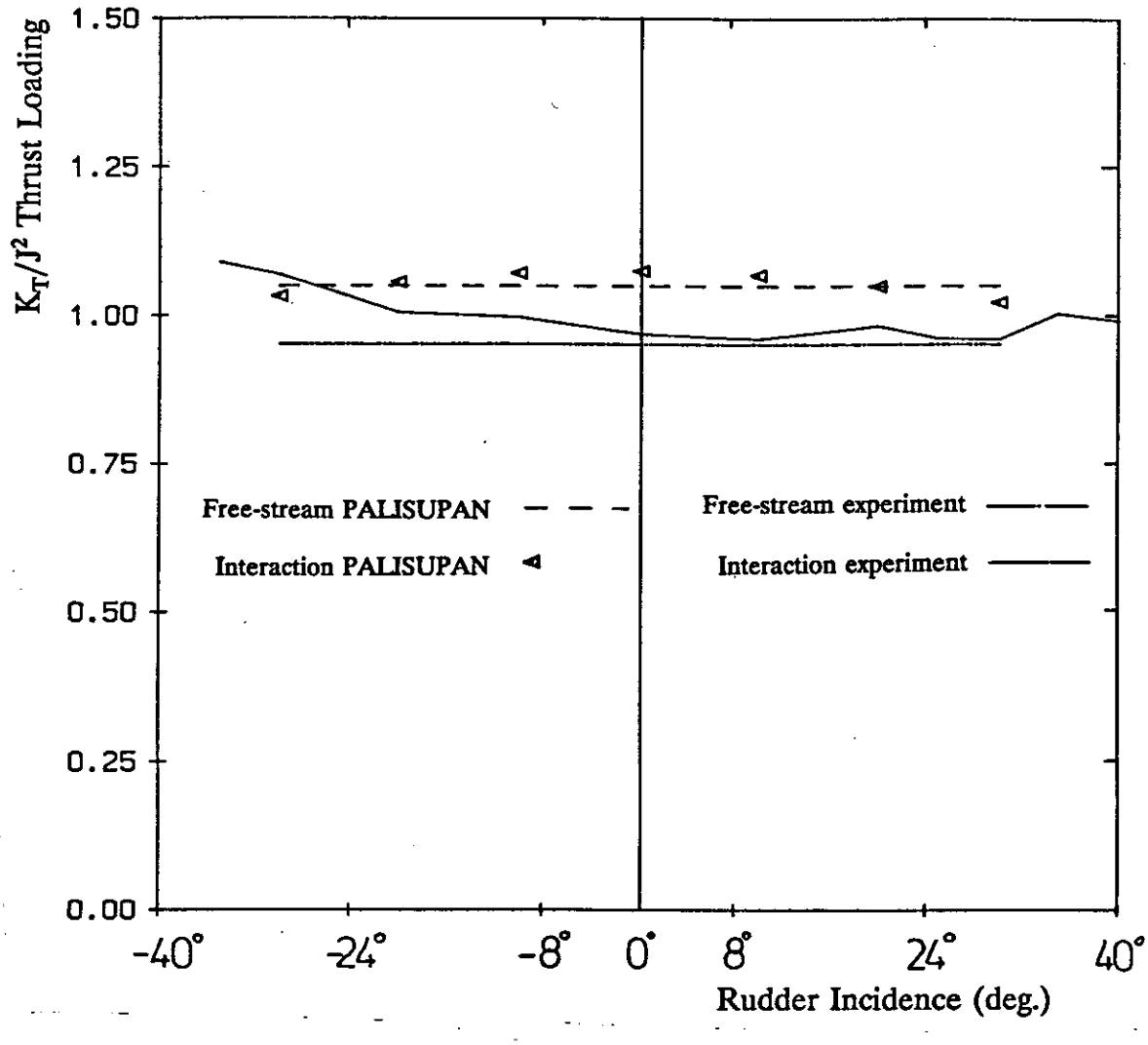

Figure 36 Variation of predicted and experimental propeller thrust loading with rudder incidence at J=0.51

Figure 36 for J=0.51. The magnitude of the increase in thrust at α=-0.4^{o} appears to be predicted well. As rudder incidence increases cross-flow effects (not modelled) at the propeller plane dominate the blockage effect of the rudder and the value of predicted propeller thrust reduces, an effect not seen in the experimental data. The limitation on the

number of panels available to model the hub and propeller has restricted the validation of the interaction effect on the propeller's performance. However, it appears that the flow effect produced on the propeller is acceptable for low values of rudder incidence ($< 10^{o}$).

7.5.8 Summary

The main aim of this validation has been to ensure that the number of panels available during the development of PALISUPAN are adequate to model rudder-propeller interaction for the prediction of rudder characteristics for use in ship manoeuvring studies.

The restrictions are acceptable as side-force is predicted within a few percent for a realistic range of propeller thrust. The limited number of empirical corrections should allow confidence in using the method for different rudder/propeller arrangements.

6 FUTURE EXTENSION OF WORK TO INCLUDE HULL EFFECTS

A ship rudder-propeller combination works in the presence of a hull. The flow over the hull influences both the inflow velocity fields of the rudder and propeller. The method developed for the interaction of the two lifting-surfaces can be extended to include the ship hull. The inflow velocity field for each body would consist of the vector sum of the interaction velocity field of the other two bodies. This has not yet been attempted. No major problems are anticipated with such an approach.

7 CONCLUSION

The lifting surface panel code has been validated against the experimental test cases for free-stream rudder and propeller and for the interaction of a rudder-propeller combination. A good comparison was obtained. It is considered that the difference between theory and experiment is due mainly to the inviscid potential approximation to the flow and the limited number of panels (400) available during the development of PALISUPAN. Other discrepancies result from the use of a time-averaged inflow velocity field and the fixed propeller wake. The latter two constraints are imposed to allow the results to be obtained

in a reasonable time and the obtained differences are acceptable. Overall, the method is a useful tool which should model parametric trends well, although an error of up to 10% in calculating rudder side-force is to be expected.

ACKNOWLEDGEMENTS

The work described in this report covers part of a research project funded by the S.E.R.C./M.o.D. through the Marine Technology Directorate Ltd. under research grant Ref No GR/E/65289.

REFERENCES

[1] Turnock, S.R., "Lifting surface panel method for modelling ship rudders and propellers". Ship Science Report No. 50, University of Southampton. 1992.

[2] Molland, A.F., & Turnock, S.R.," Wind Tunnel Test Results for a Model Ship Propeller Based on a Modified Wageningen B4.40 ", University of Southampton, Ship Science Report 46, December 1990.

[3] Molland, A.F., & Turnock, S.R.," Further wind tunnel tests on the influence of propeller loading on ship rudder performance", University of Southampton, Ship Science Report No. 52, 1992.

[4] Molland, A.F.,"A method for determining the free-stream characteristics of ship skeg-rudders", International Shipbuilding Progress, Vol. 32, No. 370, June 1985.

[5] Abbott,I.H. & Von Doenhoff, A.E.," Theory of Wing Sections", Dover Publications. 1958.

[6] Maitre, T.A., and Rowe, A.R., "Modelling of flow around a propeller using a potential based method", Journal of Ship Research, Vol 35., No. 2, June 1991, pp.114-126.

[7] Lee, J-T, "A potential based method for the analysis of marine propellers in steady flow", Ph.D. thesis, M.I.T. Dept. of Ocean Engineering, Aug. 1987.

[8] Molland, A.F.,"The prediction of rudder-propeller interactions using blade element momentum and modified lifting line theory", Ship Science Report No. 54, University of Southampton, 1992.

J WIPPELL & COMPANY LIMITED

Robemakers by appointment to the University of Southampton

PO BOX 1, 88 BULLER ROAD, EXETER EX4 1DQ. Tel: (0392) 54234

As the officially appointed Robemakers to the University, we invite you to purchase or hire the Robes you will require for the Graduation Ceremony. Please complete the attached order form, carefully checking that all details requested are recorded including payment as requested. No acknowledgement of your order or payment will be sent, but your Robes will be available for collection from our Representative in the Robing Room at the University immediately prior to the Ceremony and a receipt for your payment will be given to you then. Any payment received for Robes subsequently not required will be refunded if you advise us within 30 days following the Ceremony, and include with your request a stamped, addressed envelope. To avoid the possibility of incurring the full purchase price, Graduates are requested to return the Hired Robes to the Robing Room immediately after the Graduation Ceremony.

NEW ROBES		*GOWN*	*HOOD*	*HAT*
Bachelors/Master of Engineering	Polyester	£89.00	£41.00	£19.00
Bachelors/Master of Engineering	Russell Cord	£110.00		
Other Masters		£135.00	£57.00	£19.00
PhD Full Dress		£215.00	£44.00	£30.00
Higher Doctors Full Dress		£247.50	£55.00	£38.00

HIRING FEES	*Per Set of Gown & Hood*	*Gown Only*	*Hood Only*
Bachelors/Master of Engineering	£20.00	£13.00	£8.00
Other Masters	£21.00	£14.00	£8.00
Doctors Full Dress	£22.00	£15.00	£8.00

Hats are not required for the Graduation Ceremony, and will not be hired but may be purchased by those wishing to acquire Full Academic Dress. Full Dress Robes, less Hat, will be required for the Ceremony.